INL/RPT-22-66119
Revision 0

Advanced Graphite Creep Uncertainty Analysis

February 2022

Jason Brookman, Tommy Holschuh, Vishal Patel[a], Jorge Navarro[b], and William Windes

[a] Ultra-Safe Nuclear Corporation
[b] Oak Ridge National Laboratory

Idaho National Laboratory

INL is a U.S. Department of Energy National Laboratory
operated by Battelle Energy Alliance, LLC

Advanced Graphite Creep Uncertainty Analysis

Jason Brookman, Tommy Holschuh, Vishal Patel, Jorge Navarro, William Windes

[a] Ultra-Safe Nuclear Corporation
[b] Oak Ridge National Laboratory

January 2022

Idaho National Laboratory
INL ART Program
Idaho Falls, Idaho 83415

http://www.inl.gov

Prepared for the
U.S. Department of Energy
Office of Nuclear Energy
Under DOE Idaho Operations Office
Contract DE-AC07-05ID14517

INL ART Program

Advanced Graphite Creep Uncertainty Analysis

INL/RPT-22-66119
Revision 0

February 2022

Technical Reviewer: (Confirmation of mathematical accuracy, and correctness of data and appropriateness of assumptions.)

W. E. Windes	2/23/2022
William E. Windes ART Graphite R&D Technical Lead	Date

Approved by:

M. Davenport	2/24/2022
Michael E. Davenport ART Project Manager	Date
Gerhard Strydom	2/24/2022
Gerhard Strydom ART Co-National Technical Director	Date
Michelle Sharp	2/24/2022
Michelle T. Sharp INL Quality Assurance	Date

REVISION LOG

Rev.	Date	Affected Pages	Revision Description
0	2/24/2022	All	New Document

ABSTRACT

Uncertainty Quantification in the Advanced Graphite Creep Experiments

Jason Brookman[a], Tommy Holschuh[a], Vishal Patel[b], Jorge Navarro[c], William Windes[a]

[a]Idaho National Laboratory, PO box 1625, Idaho Falls, ID 83415, USA
[b]Ultra Safe Nuclear Corporation
[c]Oak Ridge National Laboratory

Estimating radiation damage is an important component of the post-irradiation analysis of the Advanced Graphite Creep (AGC) experiment. It depends primarily on the fast fluence, determined using well-established methods of spectral adjustment based on best estimates from models such as Monte Carlo N-Particle (MCNP), input cross-sections, and measured activities from flux wires in the experiment. However, even the most well-established "best estimate" parameter can propagate uncertainties which will affect the uncertainty in the calculated dose levels for AGC, or any experiment irradiated within a reactor. The final uncertainty estimates are only as good as the estimates of uncertainty in the inputs on which they are based. The purpose of this work is to outline some deficiencies in how these input uncertainties are presently estimated, and to outline a methodology by which they can be improved.

The fast fluence and radiation damage to graphite specimens irradiated in the Advanced Graphite Creep (AGC) experiments are presently estimated using spectral adjustment methods based on both flux wire activity measurements and MCNP model predictions. This work describes an ongoing effort to quantify and propagate uncertainties in the spectral adjustment process inputs, and thereby quantify the resultant errors in radiation damage (dpa) estimates.

The effort is multi-faceted, and we consider the impacts of both the set of flux wires selected, and the counting process. An expanded set of flux wires is identified that provides a more comprehensive data set on the fast spectrum. To address the counting process itself, a series of round-robin measurements in several reactor metrology laboratories across the Department of Energy (DOE) complex and nuclear industry are being undertaken to refine the American Society for Testing and Materials (ASTM) standards for flux wire measurements. To address the contribution of uncertainty in the MCNP model predictions, an uncertainty quantification (UQ) tool has been developed that statistically samples the model input parameters, runs a series of cases, and assimilates the results to provide an overall uncertainty.

The impact of the MCNP UQ tool results is demonstrated by re-analyzing previous AGC flux wire and irradiation data. While the expanded flux wire set obviously cannot be added to these experiments retroactively, plans for future graphite irradiations are outlined.

CONTENTS

FIGURES

TABLES

ACRONYMS & ABBREVIATIONS

AGC	Advanced Graphite Creep
ATR	Advanced Test Reactor
dpa	displacements per atom
EA	Enterprise Architecture
GRS	Gesellschaft fur Anlagen und Reaktorsicherheit
HFIR	High Flux Isotope Reactor
HPC	high performance computing
INL	Idaho National Laboratory
IRDF	International Reactor Dosimetry File
mcACE	A tool for uncertainty quantification
MCNP	Monte Carlo N-Particle (Transport Code)
ORIGEN	Oak Ridge Isotope Generation
PNNL	Pacific Northwest National Laboratory
SigPhi	σφ
TMC	Total Monte Carlo
UQ	Uncertainty Quantification
V&V	verified and validated

Advanced Graphite Creep Uncertainty Analysis

1. INTRODUCTION

The Advanced Graphite Creep (AGC) irradiation experiment has been in progress since 2006. Since then, the experiment has succeeded in providing irradiation data on graphite material properties for a number of commercial nuclear grade graphites. The AGC Experiment is irradiated within the Advanced Test Reactor (ATR) located at Idaho National Laboratory (INL) and is scheduled to continue irradiations of nuclear graphite specimens until 2026. These irradiated graphite studies are neutron dose-dependent so an accurate determination of the received neutron fluence (and neutron energy) is critical to understanding irradiation-induced material property changes for each specimen. Extensive effort has been expended within this study to quantitatively determine, via a newly developed uncertainty quantification tool, the received neutron dose for all AGC-1 specimens and the resulting uncertainty of the received dose.

The uncertainty quantification tool (labeled 'UQ tool' hereafter) conducts an uncertainty quantification (UQ) of the neutron energy spectrum based on the uncertainties of the input parameters. The Gesellschaft fur Anlagen und Reaktorsicherheit (GRS) method is used to track uncertainties through the Monte-Carlo calculations once the relevant inputs and the associated input uncertainties are established.

1.1 Dose Dependency on AGC Results

The goal of the AGC experiment is to examine the properties and behaviors of nuclear-grade graphite over a large spectrum of temperatures, irradiation fluence, and applied stress levels that induce irradiation creep strains within an high temperature reactor (HTR) graphite component. Irradiation data are provided through the AGC test series, which comprises six planned capsules irradiated in the ATR in a large flux trap at INL. The AGC irradiation conditions are similar to the anticipated environment within a high temperature core design. Each irradiation capsule is composed of more than 400 graphite specimens that are characterized before and after irradiation to determine the irradiation-induced changes in material properties and the rate of life-limiting irradiation creep for each graphite grade.

The variability, or uncertainty, of irradiated material change is well recorded, however, the uncertainty of the received dose is not as well understood. Since the material property behavior is dose dependent, determining a quantitative uncertainty in the received dose is necessary to assist in predicting the eventual material property changes for graphite or any other neutron irradiated material, Figure 1.

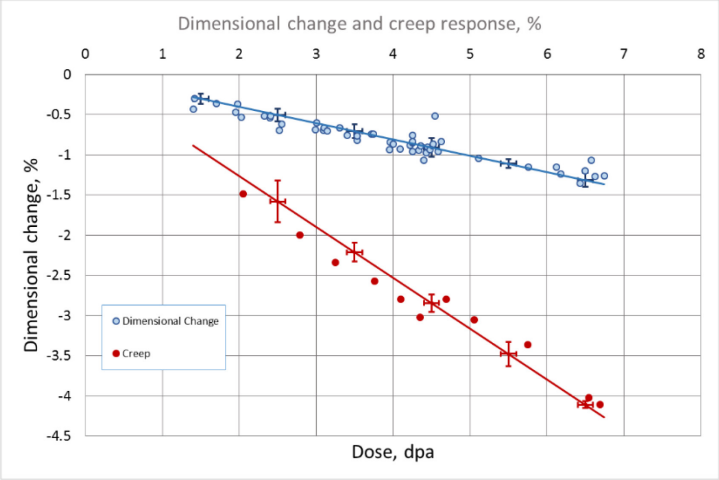

Figure 1. Irradiated material behavior data illustrating "possible" estimated uncertainty in the received dose (horizontal error bars).

The current AGC uncertainty analysis addresses the issue of uncertainty in the received neutron dose for nuclear materials irradiated within the ATR (or any other material test reactor) with a specific emphasis on the graphite specimens within each AGC-1 irradiation capsule. The desired outcome is an improved understanding of

the uncertainty of radiation damage within each irradiated graphite specimen with a quantitative analysis of the received fluence uncertainty being the optimal outcome.

1.2 Radiation Damage Estimation

Radiation damage estimation is an important component of the post-irradiation analysis of the AGC experiments. It depends primarily on the fast fluence, which is determined using well-established methods of spectral adjustment. These are based on best estimates from models (e.g., Monte Carlo N-Particle [MCNP]), input cross-sections, and measured activities from flux wires in the experiment, and they propagate uncertainties in each of these. While the methods of propagating uncertainty are well established, the final uncertainty estimates they provide are only as good as the estimates of uncertainty in the *inputs* on which they are based. The purpose of this work is to outline some deficiencies in the ways these input uncertainties are presently estimated, and to outline a methodology by which they might be improved.

The radiation damage estimates for the AGC experiments are ostensibly based on experimental data in the form of flux wire activation measurements; each AGC experiment has been instrumented with flux wires at various locations along the axial length to provide this data. However, they also depend on the results of MCNP calculations. To understand why, consider that the objective of the analysis is to estimate some number of parameters (the energy group fluences φ_j) that best reproduce the observations (the measured activities of the flux wires a_i). These are related by:

$$a_i = \sum_j \sigma_j^i \varphi_j$$

where σ_j^i are the cross sections for activation to isotope i from a neutron energy group j. Since there will be more energy groups (and hence energy group fluxes—the parameters) than flux wire activation products (the observations), the problem is under-specified, and has no unique solution. It therefore becomes necessary to supply some sort of additional information in order to solve it. The additional information typically supplied is a predicted neutron energy spectrum (e.g., from an MCNP calculation). This successfully over-specifies the problem, and a best average solution may be obtained, for example, by least-squares adjustment of all inputs (accounting properly for their uncertainty). Because the result is not a true measurement but rather an adjustment of model predictions informed by measured data, the process is referred to as "spectral adjustment."

The fluence and spectrum calculated for AGC experiments is dependent on flux wire reaction rate interpretations in conjunction with the predicted, *a priori* MCNP spectrum. In particular, for AGC experiments, relatively few flux wire activation products are available due to the physical limitations incorporating flux wires into AGC experiments. It is therefore desirable that this model be as detailed and accurate as possible (i.e., that it constitute the best available supplemental information available in order to close the problem solution). STAYSL is a code package from Pacific Northwest National Laboratory (PNNL) that uses a linear least-squares approach to "adjust" the *a priori* MCNP spectrum based on reaction rates from the flux wire activation products. The linear least-squares approach allows group-wise fluence and uncertainty values to be calculated; however, the initial MCNP spectrum must be close to true spectrum to obtain reliable results. Current work for the AGC experiments is investigating the impact of flux wire selection and *a priori* flux spectrum complexity on the final, STAYSL-adjusted spectrum.

Therefore, AGC experiments that are interpreted with flux wires cannot use simplified reactor models. While a generic fission spectrum might be sufficient to obtain an answer to the analysis, a detailed model, as faithful to the actual reactor conditions as possible, is preferred. Just such a model is developed with MCNP for experiment design as well as pre- and post-test predictions in the ATR. The predicted spectrum from this model is used as input to our least-squares adjustment in the spectral adjustment code STAYSL.

In summary, to determine the most likely value of the received fast fluence (and energy spectrum) for any AGC specimen and the overall uncertainty, the input variables for STAYSL must consist of[1]:

1. Flux wire activation measurements and the associated uncertainties,

2. A priori information of the dosimetry cross sections and the associated uncertainty (available from reference [3]), and
3. A priori information of the spectrum in the irradiation reactor and the associated uncertainty (available from the reactor MCNP model).

The code STAYSL provides a best estimate of the actual fluence and energy spectrum based on all of the above. It is this spectrum, and associated uncertainty, that is used in subsequent radiation damage calculations for all AGC-1 specimens.

STAYSL also calculates uncertainties in the group fluences based on the uncertainties in the inputs (flux wire activities, cross sections, and MCNP spectrum). STAYSL uses a specific reactor dosimetry cross section library (International Reactor Dosimetry File (IRDFF-II)) for reaction rate calculations and the subsequent flux adjustment. While uncertainties in the flux wire activities and cross sections are generally known, it is more difficult to estimate for the MCNP input spectrum. The MCNP model includes not only statistical uncertainty inherent in the Monte Carlo calculation, but also error resulting from simplifications in geometry, core fuel loading, nuclear data, densities, drum rotation and neck shim movement, among other uncertainty parameters. The total MCNP uncertainty is therefore difficult to quantify, and the present estimate for this analysis is assumed to be conservative, though it is large relative to the other sources of error. Due to this large error, the MCNP uncertainty contributes disproportionately to the overall error in the radiation damage estimate. For this reason, it is of interest to assess the MCNP uncertainty in a more rigorous and quantitative way.

2. ANALYSIS TECHNIQUES AND CODES

2.1 STAYSL PNNL and Ancillary Tools

As described above, the best estimate of the fluence and energy spectrum in an AGC experiment is determined using the STAYSL PNNL suite of codes [2] which performs a least-squares spectral adjustment. STAYSL-PNNL is an improved version of the original STAYSL code [1] which utilizes a number of additional ancillary computational tools necessary to analyze the final fluence and spectrum values. For brevity, the PNNL version of STAYSL will be understood as the version used throughout this report when STAYSL is referenced. A flow chart illustrating how input information flows through these codes, as well as a more in-depth discussion of STAYSL, can be found in [2]; also, see *Impact of Flux Wire Selection on Neutron Spectrum Adjustment* [18].

2.2 MCNP Dose Calculations

MCNP and Oak Ridge Isotope Generation (ORIGEN) are used together to calculate neutronic information through many reactor cycles and power level changes. MCNP is used to solve for neutron flux while ORIGEN is used to solve for changes in reactor materials due to neutron activation and decay. A third code, MOPY, is used to transfer information between MCNP and ORIGEN. The calculations are coupled such that there is a one-way operator split between solving for neutron flux and solving for material concentration changes. Figure 2 illustrates a schematic flow diagram of how the information and codes are used to calculate displacements per atom (dpa) in the AGC experiments.

Each input data set (represented by the arrows between boxes) has some uncertainty attached to it that should be accounted for. Once models are setup, it takes approximately 1 hour on 512 computational cores to complete each calculation.

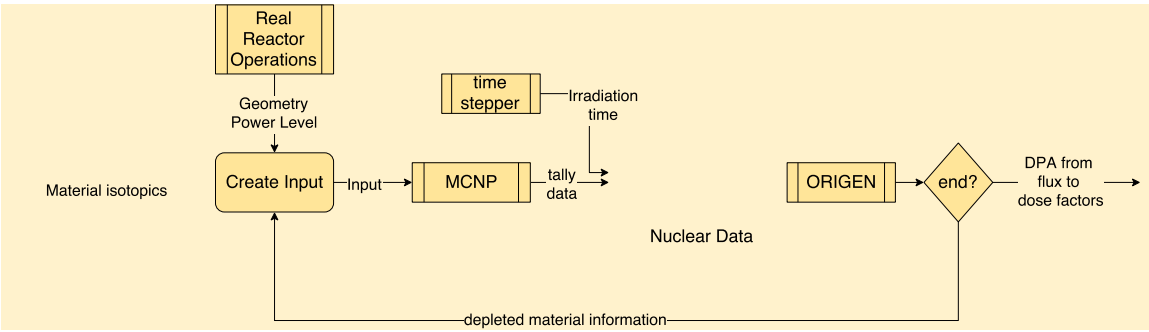

Figure 2. Calculation of dpa (displacement per atom) Flow Diagram.

This suite of tools does not possess any capability to propagate uncertainties in input parameters (only the statistical uncertainty inherent in MCNP calculations is known). The uncertainty assigned to the neutron energy spectrum predicted by MCNP has traditionally been assigned conservatively and based on expert judgement. Development of a tool to quantify such uncertainties is one of the purposes of this work, and this is described subsequently.

2.3 Application to AGC Experiments

All the AGC experiments were similarly instrumented. Each contained 26 different flux wire capsules at seven different elevations. All 26 of the vanadium capsules contained one iron wire and one niobium wire with two of the capsules additionally containing a titanium wire. There are four potentially measurable activation products from the iron and niobium wires:

- ^{54}Mn (^{54}Fe(n,p)^{54}Mn)
- ^{59}Fe (^{58}Fe(n,γ)^{59}Fe)
- ^{93m}Nb (^{93}Nb(n,n')^{93m}Nb)
- ^{94}Nb (^{93}Nb(n, γ)^{94}Nb).

The two capsules containing an additional titanium wire can provide an additional isotope, ^{46}Sc (^{46}Ti(n,p)^{46}Sc), giving potentially five isotopes for these capsules.

Three of these reactions are threshold reactions (^{54}Fe(n,p)^{54}Mn, ^{93}Nb(n,n')^{93m}Nb, and ^{46}Ti(n,p)^{46}Sc), providing information specifically about the higher end of the energy spectrum. The ^{93}Nb(n,n')^{93m}Nb reaction is particularly useful, as its threshold (~0.1 MeV) is approximately the same as the radiation damage threshold. Unfortunately, it is difficult to count; doing so requires dissolution of the wire and deposition onto a thin filter, and subsequently detecting the low energy photons emitted by its decay. This work historically has been performed at PNNL (AGC-1) but now will be conducted at INL (AGC-2 experiment and later).

The ^{59}Fe activity is apt to be lost if the wires are not removed from the experiment and counted in a timely fashion due its relatively short half-life of 45.5 days. ^{59}Fe data were collected in AGC-1 and AGC-3 but were lost in AGC-2 because of the long delay between the end of irradiation (May 5, 2012) and disassembly and counting of the wires (June–July 2014).

As noted above, corrections for self-shielding and neutron burnup are made in determining the saturated reaction rate values ($\sigma\varphi$) in the SigPhi calculator. These are typically small for the AGC experiments. In AGC-2, for example, gamma self-absorption reduces the measured activity by only ~1%, and neutron burnup varied from 3–8% depending on position.

In addition to the corrections determined by the SigPhi calculator and ancillary codes in the STAYSL PNNL suite, one additional correction has to be applied to samples measured at INL (as opposed to PNNL) to account for shielding from the vanadium capsule, from which the wires were not removed prior to counting. Based on the estimated average thickness (0.01") of the capsule based on its size and mass and mass attenuation coefficients for vanadium at the appropriate incident gamma energy, this is also a ~1% effect.

Spectral adjustment is performed with STAYSL for each sample location in the test train, using all available isotopes counted from the respective capsules. An example of the STAYSL-adjusted activities for AGC-2 is shown alongside the pre-test predictions from MCNP in Figure 3.

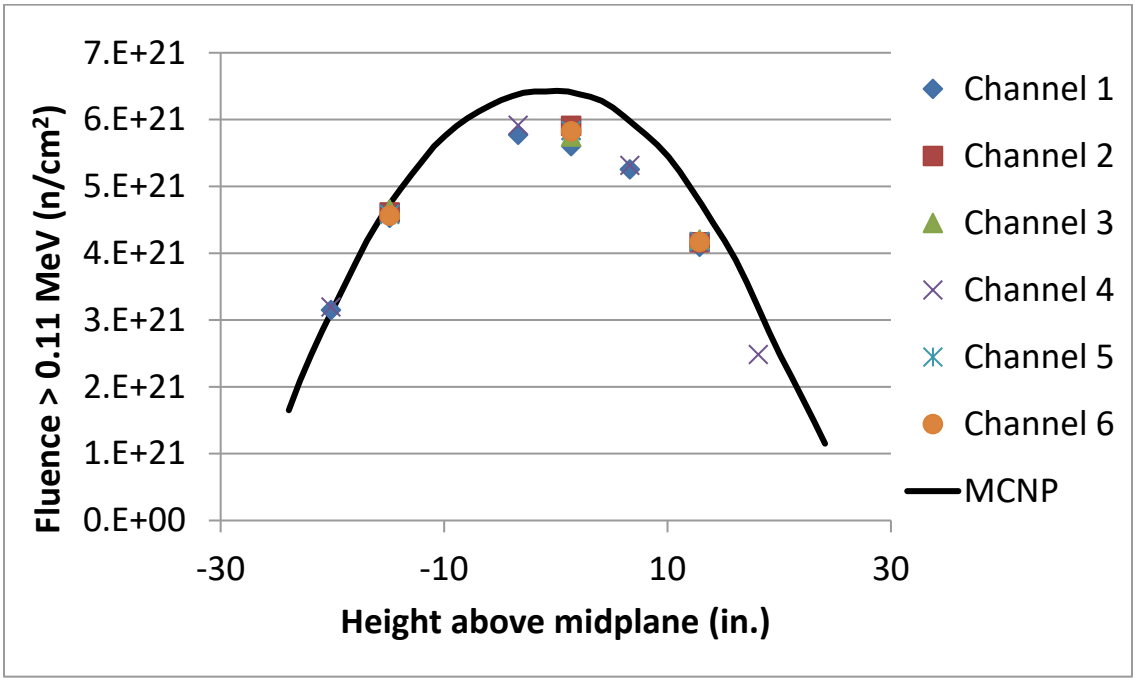

Figure 3. Fast fluence vs. position as determined from AGC-2 flux wire analysis, and comparison with pre-test MCNP predictions [4].

3. SOURCES AND DETERMINED VALUES OF INPUT UNCERTAINTIES

Uncertainties exist at every step of the calculation and measurement process used in determining the dpa dose levels in the AGC experiment. Uncertainties in each of the three inputs to STAYSL are discussed in this section, followed by a discussion of their impact on the overall uncertainty of the result.

3.1 Flux Wire Activation Measurement Uncertainties

Uncertainties in the wire activities themselves result from the counting statistics and the counting process. These vary depending on the wire material and its particular activity. Typical values for AGC-1 and AGC-2 were reported to be 2–3%, although comparative measurements undertaken as a part of this work and described in more detail below suggest the uncertainty may be larger. This uncertainty may be increased in the event of long delays before counting; it was noted above that all ^{59}Fe data was lost in AGC-2. The delay also resulted in no detection of ^{46}Sc (which has an 83.8 day half-life) in one of the capsules in which it was present, and detection with a higher uncertainty (8%) in the other.

It is presently unclear if significant error might be introduced during the necessary dissolution, deposition, and counting of ^{93m}Nb. The uncertainties reported in the measured activity of this isotope were the same as for all other isotopes in AGC-1 (2%), and this measurement was not performed for AGC-2 or ACG-3.

3.2 Nuclear Data Uncertainties

Nuclear data, such as neutron cross-sections, represent particle interaction probabilities for reactions with all nuclides present in a system. Nuclear data are created from experiments and nuclear models. As such, the nuclear data have associated uncertainties that cause uncertainties in calculations that use the data. A main input to transport codes like MCNP is nuclear data. As such, there is potential for the data to cause uncertainties in outputs.

Many nuclear data libraries exist (ENDF-B/VIII.0, JEFF-3.3, JENDL-4.0, from https://www-nds.iaea.org/) which represent best estimates for nuclear data based on various benchmark experiments and data adjustment processes. Each library contains uncertainty estimates for each cross-section, stored as covariance data. However, the covariances are generally incomplete due to lack of data or lack of need. The ENDF-B/VII.1 series and newer contain one of the most complete covariance data sets. An example of a nuclear data covariance (from https://www-nds.iaea.org/) is shown in Figure 4. In the figure, the multigroup fission cross-section is shown on the right and the percent relative deviation is shown in the top. The correlation matrix represents the inherent correlation between different energy fissions. In particular, cross-sections in correlated energy groups cannot be changed independently of one another.

MCNP can calculate sensitivities in eigenvalues via the iterated fission probability method which can, in a post-processing step, be combined with nuclear data covariances to calculate uncertainties in eigenvalues. However, MCNP cannot currently calculate sensitives in tally outputs, which are needed for the AGC graphite spectrum sensitivity. Instead, nuclear data are sampled to create random nuclear data to run MCNP many times to determine effects of nuclear data uncertainties on output. Section 4.1will discuss this in more detail.

The nuclear data library TENDL [6] creates nuclear data primarily with nuclear data models. These models have inputs from experimental work and all nuclear data generated are run through typical benchmark suites to ensure their ability to calculate benchmark quantities. This nuclear data generation framework allows for creating nuclear data with complete covariance information by varying inputs to the library generation code, then calculates output covariances. This also allows for creation of random nuclear data representative of data that agree within uncertainties to benchmark results. Random TALYS Evaluated Nuclear Data Library (TENDL) data are used in this report when relevant. Additionally, 'TALYS' is an open-source software package for the simulation of nuclear reactions.

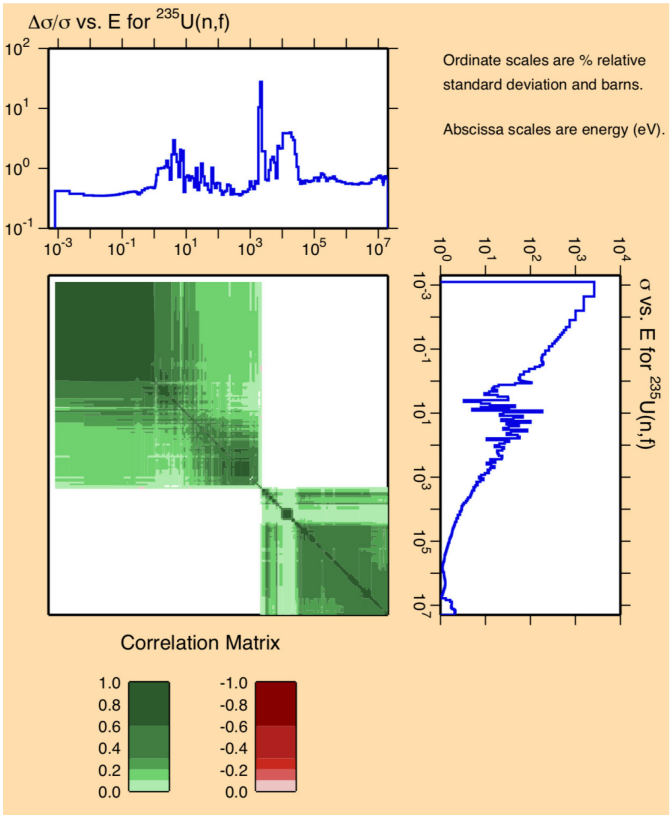

Figure 4. Example: covariance of ^{235}U fission cross section.

3.3 MCNP/ORIGEN Model Uncertainties

Because the true uncertainty in the MCNP calculation is not yet quantitatively known, values assumed in the STAYSL analysis are based on past precedent and expert judgement. The values previously ascribed to each portion of the energy spectrum are given in Table 1.

Table 1. MCNP uncertainties input to STAYSL PNNL.

Energy Range (MeV)			Uncertainty %
0	→	9.9×10^{-11}	90%
9.9×10^{-11}	→	1.0×10^{-3}	30%
1.0×10^{-3}	→	1.0×10^{-2}	20%
1.0×10^{-2}	→	1.5	15%
1.5	→	20.1	15%

The MCNP input consists of a very large number of parameters that includes the reactor geometry, material loadings, as well as operational data such as power, control drum, and neck shim positions. These parameters contain approximations or measurement uncertainties such that the relevant model outputs are uncertain. Furthermore, the actual calculation process is Monte Carlo-based, which adds another source of uncertainty.

The model uncertainty arises from model approximations and measurement uncertainties. Specifically, model approximations can lead to biases in the calculated neutron flux (energy- and space-dependent). For example, modeling the fuel assemblies as homogenized regions could increase resonance capture rates, reducing the thermal flux estimates (and thus increasing the fast flux), which implies the experiment is interacting with the wrong energy dependence in the flux. Furthermore, as-run power measurements are used to normalize lobe powers. These lobe powers determine the normalization factors for the flux within the AGC experiment, and are inputs for fuel burnup calculations. The normalization factors contribute directly to dose analysis uncertainties and the fuel burnup calculations can indirectly affect results, similar to the previously mentioned model approximation example.

3.4 Overall Uncertainty

The final result produced by STAYSL is the adjusted fluence and energy spectrum at each sample location. It produces an uncertainty associated with each of these points, which depends on the uncertainty of the inputs. From the preceding discussion, it is clear that the assumed uncertainty in the MCNP spectrum (15%) is rather larger than that in the activation measurements (typically ~2–3%). This larger MCNP uncertainty increases the overall uncertainty relative to that of the flux wire activities. The magnitude of this increase depends on the number of flux wire activation measurements taken. In AGC-1, where four isotopes were measured, the uncertainty in the fast fluence was 5–6%. In AGC-2, where only two were measured (^{59}Fe had decayed, and wires were not dissolved to count ^{93m}Nb), this uncertainty was more than 9%.

These results suggest two primary avenues for reducing the overall uncertainty: 1) better quantification of the MCNP uncertainty, and 2) an increased number of flux wire measurements. These are explored in more detail in the following section. A discussion for better quantifying the MCNP uncertainty is provided below, while details for increasing the number of flux wire measurements are explored in sections 4.1.1and 4.1.2 of reference [19].

4. IMPROVING UNCERTAINTY QUANTIFICATION

4.1 Addressing MCNP/ORIGEN Model Uncertainties

The STAYSL code takes as one of its inputs a spectrum with uncertainties to adjust. This spectrum is calculated via MCNP such that the exact experiment geometry and materials can be included to get a best estimate of the flux in the experiment. A typical MCNP spectrum output only has associated Monte-Carlo statistical uncertainty, which can be reduced to an arbitrary, sufficiently small number given enough computer time. In reality, the uncertainty is in this spectrum is larger, because almost every input to the MCNP model has associated uncertainties as described in Section 3.3. MCNP has no built-in method to calculate spectrum output uncertainties with respect to uncertain inputs. As such, an external method is used to quantify uncertainties in outputs from

uncertain inputs. This method will be described in the next section. The uncertainties calculated with this method can be used as inputs to STAYSL for spectrum adjustment that includes MCNP uncertainties.

4.1.1 The Gesellschaft für Anlagen und Reaktorsicherheit (GRS) method

MCNP does not have the built-in capability to calculate uncertainties in output spectra based on uncertain nuclear data and input parameters. However, new approaches to calculate uncertainties with Monte Carlo methods can be implemented within the current framework to propagate uncertainties from any model input. The goal of the MCNP UQ analysis is to quantitatively demonstrate how well we actually know that energy spectrum based on an analysis of the range of error for each important ATR input parameter.

The method implemented allows for uncertainty quantification of any input for any output within the MCNP/ORIGEN calculation framework that is in place. The individual codes used do not need any modification to use the new method.

A procedure, called the GRS method [8], was used to track uncertainties through the Monte-Carlo calculations once the relevant inputs and the associated input uncertainties were established. The GRS method is similar to brute force methods where simulations are run many times with inputs randomly selected and outputs stored for statistical analysis to determine uncertainties. This method does not have the drawback of running a very large number of simulations for long periods of time. Rather, a large number of simulations are run for a short time with two different random number seeds (totaling about twice the time of a single long calculation). The two different random number seeds create sets of outputs that are identically distributed such that a covariance can be computed between output sets to determine the uncertainty of the inputs. A similar method, the Fast Total Monte Carlo (FTMC) method can also be explored [9]. This method varies the random number seed for each calculation and uses different methods to deconvolve the statistical and input uncertainties. Both of these methods have been shown to agree well with a full Monte Carlo input sampling method.

Uncertainty and sensitivity analyses are performed to determine the uncertainties in the output quantities of a calculation describing a physical problem. Output uncertainties result from epistemic input uncertainties. These are due to the incompleteness of the knowledge about the input parameters (e.g., from measurement uncertainties, manufacturing tolerances). As far as nuclear data are concerned, the uncertainties mainly come from experimental errors and incomplete measurements, as well as uncertainties in physical model parameters. When applying random sampling methods for the uncertainty analysis, as implemented, for example, in the GRS Software for Uncertainty and Sensitivity Analysis (SUSA) code package [1], normally deterministic codes are used for solving the physical problem. For steady-state neutron transport in complex geometrical arrangements however, Monte Carlo codes are best suited for describing the problem by a direct simulation of the microscopic processes, because practically no geometry simplifications are necessary.

The application of the Monte Carlo method as transport solver introduces an additional kind of uncertainty to the calculation results—the randomness of the calculation procedure performed by the Monte Carlo sampling process ("aleatoric uncertainty"). In "well-behaved" situations, this aleatoric sampling output uncertainty can be reduced or even eliminated by increasing the number of sampled neutron histories in the calculation. In Monte Carlo reference calculations (i.e., without taking epistemic input uncertainties into account), the number of neutron histories is chosen so the resulting aleatoric uncertainty of the output quantity under consideration, mostly expressed by variance or standard deviation, is below a desired value. When conducting sampling-based uncertainty analyses, the complete batch of calculations is usually performed with the same high number of neutron histories in each of the calculation runs. Further effort to separate aleatoric and epistemic sampling uncertainties is unnecessary, and the usual one-dimensional sample-based epistemic uncertainty analysis can be performed.

The transport calculations are repeated many times with sampled nuclear data, and the results are statistically analyzed. This leads to the quantification of uncertainties of arbitrary output quantities and, to a certain degree, to quantification of sensitivities with respect to the uncertain input parameters.

The GRS method can be performed as follows:

1. n calculations with m/n histories, each using different $A_{i=1\ldots n}$ (A representing a set of randomly varied inputs) and a unique seed s_1. A given distribution for the calculated quantity is obtained: $q^{i=1\ldots n}$.

2. n other calculations with m/n histories, each using different $A_{i=1\ldots n}$ [similar to case (1)] and a unique seed s_2. A given distribution for the calculated quantity is obtained: $q^{i=1\ldots n}$
3. The covariance between calculations (1) and (2) is equal to the variance due to $\vec{A}$: $cov\left(q^{(1)}, q^{(2)}\right) = \sigma_A^2(q)$.

Implementing this GRS method will allow for uncertainty quantification of any input for any output within the MCNP/ORIGEN calculation framework. The individual codes used do not need any modification to use the new method.

The two random seed file sets allow for the generation of two series of calculations, and computation of the sample covariance of the two-dimensional analysis. N simulations with different input s are run for a short time with a single random number seed, then each N simulation is reran with a different random number seed (totaling about twice the runtime of a single long calculation). The two different random number seed simulations have identical aleatoric Monte Carlo (MC) uncertainty distributions. The covariance of the output sets is the epistemic uncertainty of the varying inputs because the MC uncertainty is almost eliminated (goes to zero as MC sample batch sizes increases). The GRS method relies on the statistical distribution of MC outputs to determine input uncertainty. By taking two sets of random simulations, two distributions with the same uncertainties are found. The covariance of these distributions is the input uncertainty because statistical errors are the same in both sets and are removed by the covariance operation.

From one series of long runs, the evaluated total combined uncertainties are much larger than the epistemic uncertainties alone, determined from the series of long runs. However, by using two series of short runs with different Monte Carlo random numbers—as described above—the determined uncertainties are in very good agreement with those from the series of long runs. See reference [1] for a detailed analysis of this assertion.

4.1.2 mcACE: Software for MCNP Uncertainty Quantification

The GRS method requires creation of hundreds of MCNP inputs as well as parsing and storing of relevant outputs. mcACE is a tool developed to perform UQ and handle data management. mcACE allows for sampling of any part of an MCNP input from random distributions to determine output uncertainties based on those inputs. It also handles data post-processing, data transfer, MCNP/ORIGEN coupling, and performs statistics on relevant results. The typical workflow is shown in Figure 5 and it involves describing the relevant uncertain inputs in the mcACE input file, then running the code [10].

mcACE assumes the input model is validated. However, the UQ steps need to be verified. Unit tests have been created for input manipulation, data parsing, and statistics. Verification of the GRS method was performed by running 500 long-running MCNP calculations where nuclear data were varied and the ATR fuel spectrum in a fuel element axial slice was calculated. The uncertainty from the input is calculated using the Total Monte Carlo (TMC) method as,

$$\sigma^2_{observed} \approx \sigma^2_{input} + \overline{\sigma^2_{statistical}}$$

$$\overline{\sigma^2_{statistical}} = \frac{1}{N}\sum_{j=1..N} \sigma^2_{statistical,j}$$

with parameters defined in Table 2. This requires a considerable runtime, often 30 times as long as a GRS run. However, the reasoning behind calculating input uncertainty is straightforward—if TMC and GRS agree, the GRS method implemented can be considered verified.

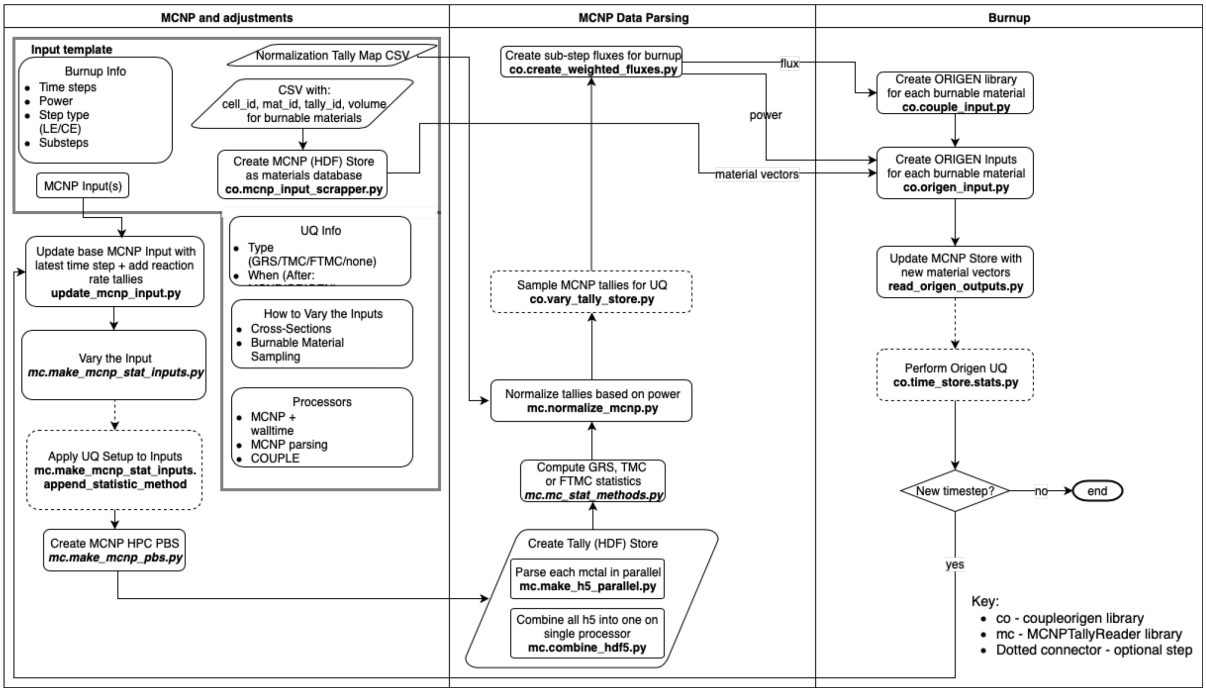

Figure 5. mcACE workflow.

Figure 6 compares GRS and TMC relative uncertainties in an energy-dependent spectrum in an axial level of an ATR fuel element. The TMC case was run with 20 times more runtime for well-converged results. For relative errors less than 0.6, it can be seen that TMC and GRS agree very well. For higher relative errors, the two methods agree within 10%. These differences are likely due to energy bins in the flux that have very low values and as such are not as well converged as other bins. The observed good agreement verifies the use and implementation of GRS for UQ in the ATR model.

Table 2. TMC Equation Description.

Quantity	Description
$\sigma^2_{observed}$	The observed variance of outputs
σ^2_{input}	The input variance that is being calculated
$\overline{\sigma^2_{statistical}}$	The average statistical variance of the outputs
N	The number of outputs
$\sigma^2_{statistical,j}$	The statistical variance of an individual output

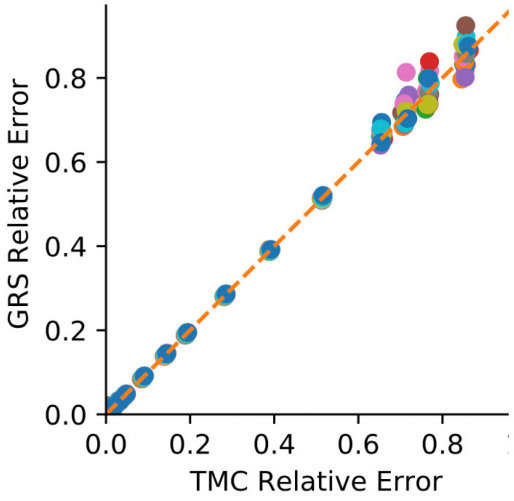

Figure 6. Relative uncertainty in the ATR energy spectrum compared using TMC vs. GRS with 20× less runtime.

5. ATR SENSITIVITY STUDY

5.1 Overview

The sensitivity analysis of ATR consisted of using mcACE to determine numerous uncertainties associated with various input parameters. For each of these, a single UQ run was conducted while varying only the single parameter being evaluated, leaving all other factors of the ATR model alone. Subsequently, all the selected parameters were varied simultaneously for determination of combined effects.

The parameters varied were the following:

- Fuel densities
- Fuel volumes
- Fuel enrichments
- Uranium cross-sections (given tables)
- Control element positions
- Beryllium density and volume in ATR
- Aluminum density and volume in ATR.
- Fuel burnup isotopes and associated cross-section files.

The MCNP model consisted of seven axially positioned tallied markers within the South Flux Trap of the ATR, in accordance with the location of flux wires in the AGC-1 irradiation experiment. A standard MCNP input model describing the average core loading during the first cycle of the AGC-1 irradiation was employed for the parameters analyzed. Seven input parameters were analyzed to determine the errors associated with the AGC-1 experiment, with inputs varied simultaneously for determination of combined effects. Neutron flux tallies in the MCNP6 input deck were incorporated into the South Flux Trap at the axial locations of flux wires within the AGC-1 experiment (see Table 3), for a direct correlative analysis through the use of STAYSL.

Table 3. Locations of AGC-1 flux wires and corresponding MCNP axial tallies.

Elevation of Wires from Core Centerline (in.)	Elevation of Wires from Core Centerline (cm)
18.5	46.99
12.5	31.75
7	17.78
2.25	5.72
–7.25	–18.42
–13.75	–34.93
–21.25	–53.98

5.2 MCNP

5.2.1 Computer Code Validation

The computer code MCNP is listed in the INL Enterprise Architecture (EA) Repository as qualified scientific and engineering analysis software for neutronic analyses to support irradiation experiment design and analysis calculations (see EA Application ID 234728). Table 4 lists the version and EA Software ID for the computer code used to perform the calculations and analyses documented by this report.

Table 4. INL Qualified Analysis Software, Version, and EA ID.

Code Name	Version	EA Software ID
MCNP	6 (Release 1.0) [11]	336729 397392 [11][12]

MCNP has been verified and validated (V&V) for use at INL consistent with the MCNP Version 6, Release 1.0 software management report [14]. The MCNP Version 6, Release 1.0 V&V process [14] was performed and accepted on the Falcon high-performance computing (HPC) system at INL.

This research made use of the resources of the HPC Center at INL, which is supported by the Office of Nuclear Energy of the U.S. Department of Energy and the Nuclear Science User Facilities under Contract No. DE-AC07-05ID14517. The computer configurations listed in Table 5 were used to perform the MCNP calculations reported here. Evaluations are performed after each HPC outage [12] to show the V&V results have not been effected by system upgrades.

5.2.2 Input Deck

The MCNP file used for the UQ tool analysis incorporated the average core loading (cylindrical shim positioning, neck shim positioning, and fuel loading), including experiment loading, to describe the first cycle of the AGC-1 irradiation. The model consisted of the AGC-1 experiment within the South Flux Trap, with tallies at locations to match the placement of flux wires in the AGC-1 experiment (see Table 3). The first cycle of the AGC-1 experiment, cycle 145A, was irradiated for 54.7 days (09/05/2009-11/06/2009) with as-run averaged lobe powers of 18.0-17.9-23.2-23.8-25.7 (NW-NE-C-SW-SE). See Engineering Calculations and Analysis Report (ECAR)-1406 [13] for AGC-1 details and as-run results prior to the UQ analysis.

Table 5. Computer Configurations for INL Qualified MCNP5/6 and ORIGEN2 Installations.

Computer	Processor/Hardware	Operating System

34,992 core SGI ICE X distributed memory cluster (Falcon computer system)	Two service nodes acting as login nodes each with: • Two 18 × 2.1 GHz Xeon E5-2695 v4 Broadwell chipset • 64 Gigabytes (GB) of shared memory per node • Fourteen Data Rate (FDR) InfiniBand interconnect network 972 compute blades with: • Two 18 × 2.1 GHz Xeon E5-2695 v4 Broadwell chipset • 64 GB of shared memory per node • FDR InfiniBand interconnect network	SUSE Linux Enterprise Server 11 SP4

The kcode used was as follows:

kcode 7500 1.005 50 10000,

where 7500 describes the number of particles per generation, 1.005 becomes the beginning eigenvalue, skipping 50 cycles before running an additional 9950. MCNP reported converged Shannon entropy within 15 cycles such that skipping 50 cycles was appropriate.

The primary goal of using the UQ tool was to compute a neutron energy spectrum and relative errors at each flux wire location within the AGC-1 model; as such, seven graphite tallies of 4-cm height with a diameter of 0.6 cm, were described as follows in the MCNP deck Figure 7:

```
c UQ Tallies
c
fc4 Neutron Flux
f4:n
c
c SFT Position
c Tallies
     25047                                $ A5 Graphite Tally 7 107.950
     25046                                $ A5 Graphite Tally 6  92.710
     25045                                $ A5 Graphite Tally 5  78.740
     25044                                $ A5 Graphite Tally 4  66.675
     25043                                $ A5 Graphite Tally 3  42.545
     25042                                $ A5 Graphite Tally 2  26.035
     25041                                $ A5 Graphite Tally 1   6.985
c
fq4    e f
e4    1.000e-10 1.0000e-9 1.0000e-8 2.3000e-8 5.0000e-8 7.6000e-8 1.1500e-7
      1.7000e-7 2.5500e-7 3.8000e-7 5.5000e-7 8.4000e-7 1.2750e-6 1.9000e-6
      2.8000e-6 4.2500e-6 6.3000e-6 9.2000e-6 1.3500e-5 2.1000e-5 3.0000e-5
      4.5000e-5 6.9000e-5 1.0000e-4 1.3500e-4 1.7000e-4 2.2000e-4 2.8000e-4
      3.6000e-4 4.5000e-4 5.7500e-4 7.6000e-4 9.6000e-4 1.2750e-3 1.6000e-3
      2.0000e-3 2.7000e-3 3.4000e-3 4.5000e-3 5.5000e-3 7.2000e-3 9.2000e-3
      1.2000e-2 1.5000e-2 1.9000e-2 2.5500e-2 3.2000e-2 4.0000e-2 5.2500e-2
      6.6000e-2 8.8000e-2 1.1000e-1 1.3500e-1 1.6000e-1 1.9000e-1 2.2000e-1
      2.5500e-1 2.9000e-1 3.2000e-1 3.6000e-1 4.0000e-1 4.5000e-1 5.0000e-1
      5.5000e-1 6.0000e-1 6.6000e-1 7.2000e-1 7.8000e-1 8.4000e-1 9.2000e-1
      1.0000e+0 1.2000e+0 1.4000e+0 1.6000e+0 1.8000e+0 2.0000e+0 2.3000e+0
      2.6000e+0 2.9000e+0 3.3000e+0 3.7000e+0 4.1000e+0 4.5000e+0 5.0000e+0
      5.5000e+0 6.0000e+0 6.7000e+0 7.4000e+0 8.2000e+0 9.0000e+0 1.0000e+1
      1.1000e+1 1.2000e+1 1.3000e+1 1.4000e+1 1.5000e+1 1.6000e+1 1.7000e+1
      1.8000e+1 1.9000e+1 2.0000e+1
```

Figure 7. AGC-1 MCNP Input deck information.

All cells describing the fuel surface cards, the fuel material cards, and the aluminum cells throughout the core, plus the beryllium cells throughout the core as well as the drum (control element) cells, were detailed appropriately within the UQ tool for manipulation of the analyzed input parameters.

5.3 Input Parameter Uncertainties

Fuel enrichment error: Data at the 95% confidence level show that the method used to assign U-235 enrichment values have a bias of less than 0.2% relative, but with a maximum allowable window up to 0.7%. For a conservative analysis, we used the latter error margin of 0.7% for our input error ([14], page 29).

Control shim angle error: Control drum movements were varied ±1.5 degrees. Very little information is available on this parameter. Two separate analyses were conducted with the drums varied with an error of ±1.5

degrees and $\pm$5.0 degrees. Due to the difference in this study being minimal, an assumed value of $\pm$1.5 degrees was employed within the UQ tool.

Uranium cross-section errors: The uranium cross-sections are randomly varied from TALYS through TENDL libraries, providing 740 random Uranium nuclear data files. Model parameters, such as for the TALYS code, are randomly varied following given parameter covariances. This produces random nuclear data. These random nuclear data are either averaged to produce a covariance file, or directly formatted into nuclear data libraries to be used in a Monte Carlo process (leading to the TMC method). The same MCNP input files are used together with the same version of MCNP6.1 (MCNP6 Users manual-Code version 6.1.1beta, 2014). Similarly, the same version of NJOY (12.21 MacFarlane and Kahler, 2010 [15]) is used to process the evaluated nuclear data file (ENDF)-6 files into the ACE (A Compact ENDF) format. The so-called ‘‘ENDF-6” format, as defined in reference Trkov et al. (2012) [16], is the basic format used to create and share the nuclear data quantities. ‘NJOY99 update 396’ was used for all isotopes [17]. Additionally, the NJOY Nuclear Data Processing System is a modular computer code designed to read evaluated data in ENDF format, transform the data in various ways, and output the results as libraries designed to be used in various applications.

Aluminum density error: The density of Al-6061 is typically given to be 2.70 $\frac{g}{cm^3}$. This parameter was selected due to the large quantity of aluminum throughout the core; an error of 0.01 $\frac{g}{cm^3}$ (and rounded up to 0.4%) was assumed for this parameter.

Beryllium density error: The density of beryllium S200F produced by Materion, making up the reflector and control shims in the ATR, is given to be 0.067 $\frac{lbs}{in^3}$ (1.855 $\frac{g}{cm^3}$). The beryllium density for the ATR is at least 99.7% of theoretical density, determined using the water displacement method. The theoretical density is calculated using the following equation:

$$Theoretical\ Density\ \left(\frac{g}{cm^3}\right) = \frac{100}{\frac{100 - \%BeO}{1.8477\ \frac{g}{cm^3}} + \frac{\%BeO}{3.009\ \frac{g}{cm^3}}}$$

The vacuum hot pressed material used in the ATR reflectors has a density no lower than 99.7% of the theoretical value, which allows us with confidence to place the error at $\pm$0.005 $\frac{g}{cm^3}$ (or 0.3%).

Fuel density error: Per section 3.5.2.1 of [14], page 15, the error in the fuel density was determined to be 0.465%. Although it is stated that the fuel mass of each fuel element is 1075 $\pm$10 grams, in practice this value has never exceeded $\pm$5 grams, which gives a fuel mass error of $\frac{5}{1075} = 0.00465$ grams (or 0.465%). This mass error, rounded up to 0.5%, is used as the input error for fuel density.

Plate thickness error (or error in fuel volume): It turns out that this simply becomes a mass problem, delineated above. Each plate is formed from a precise amount of powder. Although throughout the rolling and annealing process each plate (the fuel portion) may in principle become non-uniform in its thickness, the variation in the amount of fuel per plate is directly dependent upon the mass error stated above. This analysis employs an MCNP model that describes the fuel as three radial and seven axial zones to represent the ATR fuel elements. However, for a conservative estimate of this ATR core parameter, we did vary the fuel volume by 0.1%.

Burnup: A burnup analysis was rigorously analyzed to gather the associated errors across multiple timesteps and cycles. The fuel actinide and isotopic buildup within the 40 fuel elements per timestep (three timesteps per cycle: beginning, middle, and end) were tracked. Each element was relocated within the core as fuel shifting occurred and new fuel elements were introduced. This was conducted in MC21, and then a script was written to translate the results to MCNP. See 10 for the full list of fuel isotopes investigated.

The uncertainty in the spectrum due to burnup was accomplished (the approach is detailed below), and 240 isotopes were decided upon due to the isotopes tracked by ATR and MC21 (See ‘Appendix B Burnup Sensitivity Parameter—Fuel Isotopes Investigated’ for the full list of isotopes). Note that a handful of isotopes (H3, He2, He3, Li7, N14, O17, Cr54, Eu155, Dy163, Th232, U236, Pu241) were also not analyzed because of issues with pushing them through the ASAPy (A Simple ACE Python editor) program or the final UQ run. As such, they

are not in the Appendix B list. The Evaluated Nuclear Data File (NDEF) files for each of the isotopes were gathered and the steps below were followed to translate them into ace format, from which random cross-section samples per isotope were gathered via a secondary process (detailed below).

As discussed in Section 3.2: The nuclear data library TENDL [6] creates nuclear data primarily with nuclear data models. These models have inputs from experimental work and all nuclear data generated are run through typical benchmark suites to ensure their ability to calculate benchmark quantities [17]. This nuclear data generation framework allows for creating nuclear data with complete covariance information by varying inputs to the library generation code, then calculating output covariances. This also allows for creation of random nuclear data to represent data that agree within uncertainties to benchmark results. Random TENDL data is used in this report when relevant.

Openmc and NJOY2016 can be used in unison to convert ENDF/TENDL cross-section libraries per isotope to ace format. Using the original ENDF data and the created ace data, ASAPy can generate random data. From here, the perturbed files per isotope were added to the cross-section directory to be called upon by the UQ tool via the mcACE.ini file, with the isotopes appropriately labeled and added to the mcACE.ini file. Last, the isotopic content of the fuel detailing all isotopes listed in 'Appendix A—Burnup Sensitivity Parameter Fuel Isotopes Investigated' (tracked by ATR at INL) were gathered from MC21 files that described the beginnings, middles, and ends of numerous AGC-1 irradiation cycles. This allowed us to determine which time within a cycle leads to the highest uncertainty in the spectrum due to fuel burnup and isotopic content. From this, established fuel scenarios were added to the other uncertainty parameters (e.g., fuel enrichment, beryllium density, aluminum density) for a final analysis.

5.4 Bounding Uncertainty Approach

Numerous timesteps across three cycles of the AGC-1 irradiation were performed with the UQ tool to gather the bounding uncertainty. A handful of the seven sensitivity parameters changed throughout each of the cycles analyzed: fuel isotopics, drum and neck shim positions. These bounding data tables were fed to the flux wire analyst for use in STAYSL.

6. RESULTS

6.1 UQ Tool

The total flux uncertainties in the AGC graphite from the UQ run that included all seven input parameters are provided in Table 6. An example of the output data gathered from a UQ run is shown in Figure 8, and the data itself can be found in Appendix B. This result is averaged over all seven graphite samples and is zoomed to the approximate graphite neutron damage threshold of 0.1 MeV. The relative uncertainty is small (~1–2%) up to about 1 MeV, then the relative uncertainty increases. The total error value is also shown since the relative uncertainty can be misleading, as an extremely uncertain flux with very small magnitude will not have much of an effect on the STAYSL calculation.

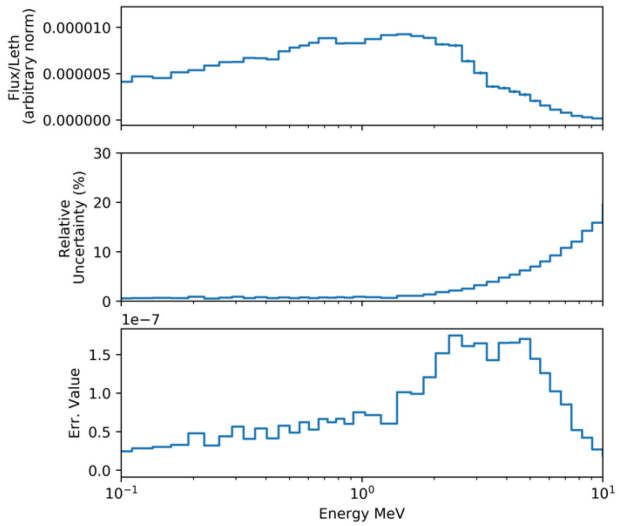

Figure 8. Spectrum uncertainties with all studied parameters varied.

Table 6. Total uncertainty percentages vs axial flux wire location.

Distance from Core Midplane (in)	-53.98	-34.93	-18.42	5.72	17.78	31.75	46.99
Uncertainty Percentages	0.9557	0.8074	0.7486	0.8530	0.9314	1.0213	1.3235

The relatively small uncertainties calculated imply that the spectrum is not particularly sensitive to the inputs that were varied. This is typically ascertained via a sensitivity analysis; however, the GRS method can only quantify uncertainties, not predict sensitivities.

To calculate sensitivities, the full calculation is repeated varying only one parameter at a time. Figure 9 shows two single parameter runs compared with the full seven parameter run. The two parameters shown are the uranium cross-sections and enrichment. The fact that the uranium cross-section run is very similar to the full seven parameter run shows that most of the calculated uncertainty in the latter comes from the uranium cross-sections. The enrichment contributes a small amount of uncertainty relative to the cross-sections. These single parameter runs also show that there are potential correlations between outputs for the varied parameters because the individual uncertainties do not add up to the case where all parameters are varied. There is also a potential for small numerical uncertainties of the actual predicted uncertainties. This can be shown with a convergence plot by only including a few sampled energies at a time in the GRS scheme, as seen in Figure 10. The uncertainty results are seemingly converged; however, there are clearly some fluctuations. That variance can be considered negligible due to its small size.

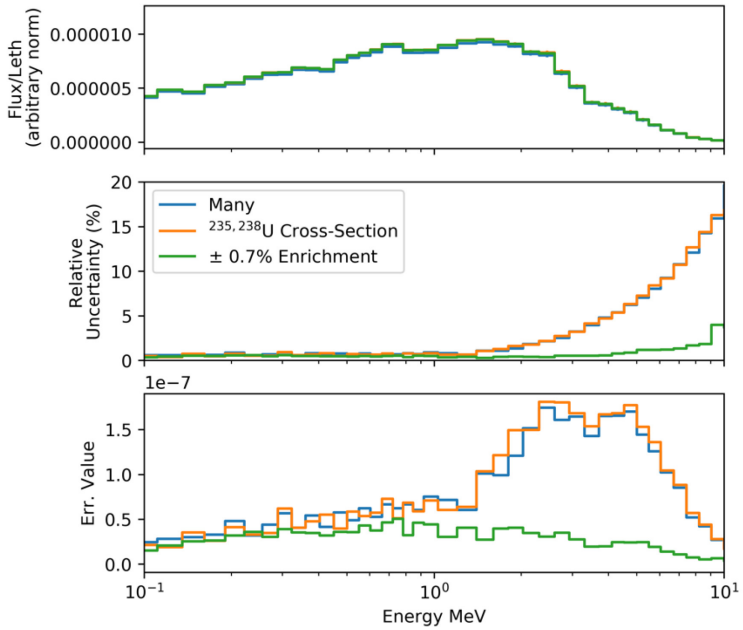

Figure 9. Single parameter variation results.

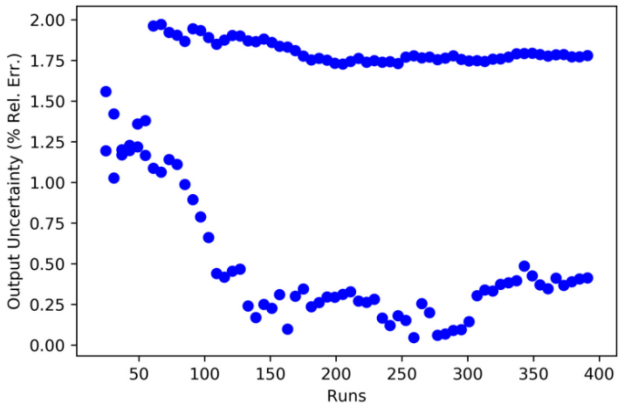

Figure 10. Convergence behavior of two energy bins (1.4 MeV top and 0.019 MeV bottom) using the uranium cross-sections single parameter variation case.

An additional UQ run was conducted, varying all the input parameters described above with the input error doubled for each parameter (except the uranium cross-sections). The overall uncertainty values changed very little in this case, further corroborating the original results that the uranium cross-section dominates the uncertainties in the other six parameters investigated.

All data were fed to the flux wire analyst for adjustment with STAYSL. Concomitant with each of the seven axial tallies were a flux value and its associated error in 100 energy groups.

6.2 Spectral adjustment with STAYSL

To examine the influence of the mcACE uncertainty result on the best estimate, and associated uncertainty resulting from spectral adjustment with STAYSL, the AGC-1 flux wire data were re-analyzed. AGC-1 was selected for this purpose because it possesses the most comprehensive set of activation product measurements, and these are assumed to have less uncertainty than subsequent AGC experiments. Two variations were run, each making use of the exact same:

- Flux wire activation measurements and uncertainties

- Cross section data and uncertainties (IRDF)
- MCNP neutron energy spectra.

The latter were obtained from the re-analysis of AGC-1 described in the preceding section.

In the two sets of analyses, the only aspect that differed was the uncertainty in the MCNP spectra. Case 1 used the existing, relatively large uncertainty bounds, 15% in the fast spectrum. Case 2 made use of the uncertainty from the mcACE analysis for each of the 100 energy bins, which was on the order of 1–2% up to ~1.5 MeV, increased to ~15% at about 5 MeV, and increases farther from there to ~35% at 10 MeV. The resultant radiation damage estimates and uncertainties are summarized in Table 7.

Table 7. STAYSL results for AGC-1, with large (Case 1) and small (mcACE, Case 2) uncertainty.

Sample ID	Channel	Elevation (in) from core center	Case 1		Case 2		Relative Change in DPA From Case 1 to Case 2
			dpa	Relative uncertainty	dpa	Relative uncertainty	
2	1	18.5	3.39	6.56%	3.27	2.53%	–3.43%
3	1	12.5	5.06	6.58%	4.90	2.39%	–3.32%
4	1	7	6.82	6.51%	6.08	2.49%	–10.92%
8F	1	2.25	6.36	5.93%	6.12	2.45%	–3.79%
6	1	–7.25	7.04	6.56%	6.22	2.50%	–11.76%
7	1	–13.75	5.77	6.56%	5.43	2.46%	–5.85%
F	1	–21.25	3.35	6.49%	3.10	2.62%	–7.43%
H	2	12.5	5.10	6.58%	4.92	2.39%	–3.48%
I	2	2.25	7.41	6.56%	6.75	2.46%	–8.97%
J	2	–13.75	6.45	6.49%	5.87	2.50%	–8.94%
K	3	12.5	5.00	6.59%	4.88	2.38%	–2.41%
N	3	2.25	6.37	6.62%	6.40	2.37%	0.50%
O	3	–13.75	5.78	6.54%	5.59	2.44%	–3.32%
S	4	18.5	3.25	6.57%	3.21	2.51%	–1.29%
T	4	12.5	4.99	6.58%	4.92	2.38%	–1.38%
V	4	7	6.55	6.54%	5.88	2.48%	–10.19%
U8	4	2.25	7.17	6.23%	6.79	2.42%	–5.21%
X	4	–7.25	7.21	6.52%	6.76	2.45%	–6.33%
XX	4	–13.75	6.33	6.49%	5.94	2.47%	–6.27%
Y	4	–21.25	3.27	6.48%	3.07	2.60%	–5.86%
CK	5	2.25	7.49	6.56%	6.82	2.46%	–8.83%
CE	6	12.5	5.57	6.51%	5.22	2.42%	–6.21%
CA	6	2.25	6.83	6.55%	6.62	2.41%	–3.15%
CH	6	–13.75	6.05	6.52%	5.65	2.47%	–6.50%

The first and most obvious result of using the mcACE uncertainty is a reduction in the adjusted uncertainty, from about 6.5% to about 2.5% in each case. This reflects the much lower uncertainty predicted by mcACE for that part of the fast spectrum in which the fluence is highest (< 5 MeV).

However, it would also appear that not just the uncertainty, but the *results themselves* changed as a result of application of the mcACE uncertainties—the displacements per atom (dpa) value is decreased relative to Case 1 for all but one sample (N, which has an increase of 0.5%), in a few cases (4, 6, and V) by more than 10%. That the two results are indeed different (i.e., the differences are not simply a result of uncertainty) can be established by

statistically testing the null hypothesis that they are the same (i.e., that the mean μ_d of the differences between the dpa values is zero). For this purpose, we use the Student's t test, for which the test statistic is

$$t = \frac{\bar{x}_d - \mu_d}{\frac{s_d}{\sqrt{n}}}$$

Here $\bar{x}_d$ is is the mean of the sample differences (Δdpa for each sample), s_d is the standard deviation of those differences, and $n = 24$ is the sample size. The resultant test statistic is $t = -6.965$, corresponding to a p-value (for a two-tailed test) of 4.24e-7 (i.e., we can say with >99.99995% confidence that the two analyses indeed produce fundamentally different results).

As previously, it is instructive to look at a representative graph of the input and adjusted spectra to understand, at least partly, why the difference occurs. These are shown for sample 6 (which exhibited the greatest difference) in Figure 11. In Case 1, a significant (upward) adjustment of the fast spectrum occurs resulting from the flux wire activation measurements. In Case 2, using the significantly reduced uncertainties indicated by the mcACE analysis, this effect is very minimal, and the two spectra are little different from one another. The apparent impact of the lower uncertainties is to increase the importance of the MCNP spectrum in the adjustment, to the point that the (many fewer) activation measurements have little impact on the shape of the spectrum (i.e., that this is influenced primarily in Case 2 by the MCNP result, not the measured data).

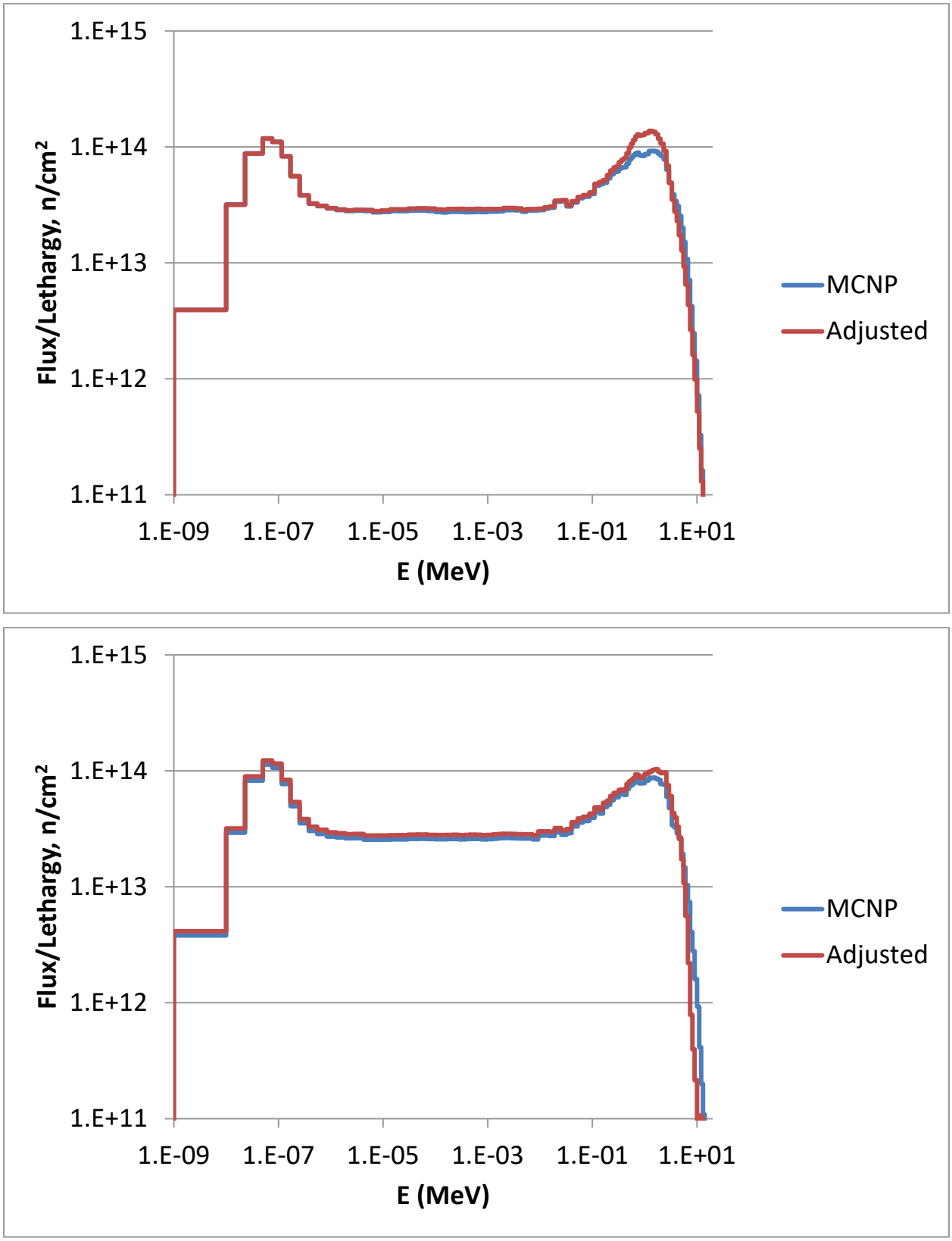

Figure 11. Input and adjusted spectra for AGC-1 sample 6 for Case 1 (top) and Case 2 (using uncertainties from the mcACE analysis, bottom).

7. SUMMARY AND CONCLUSIONS

Motivated by a need to better quantify the uncertainty in property changes in graphite irradiated in the AGC experiments, we have outlined a number of efforts to more rigorously quantify the uncertainty in the radiation damage estimates on which these depend. Such estimates are made using a code called SPECTER, which computes dpa based on radiation damage cross sections and an input neutron fluence and energy spectrum. The latter results from a spectral adjustment calculation, performed here using the STAYSL code. STAYSL performs a least-squares fit of the neutron energy spectrum to flux wire activation measurements, using cross sections provided by the IRDF library, and supplemented by a normalized spectrum calculated by MCNP. The latter is necessary because the spectrum is divided into many more energy groups (100) than there are flux wire activities; it serves to close the problem, which would otherwise be underspecified. The fitting performed by STAYSL appropriately weights all of the activation measurements, cross sections, and MCNP group fluxes according their uncertainties, and propagates these to quantify the uncertainty on the final, adjusted spectrum. The cross section uncertainties are provided with the libraries and were not considered any further in this work, which is focused on refining the uncertainty in the flux wire activities and the MCNP spectrum which were added to STAYSL.

Estimates of the true uncertainty in the MCNP spectrum have historically been rough estimates, or were intended to be bounding values only. As a part of this effort, a UQ tool mcACE has been developed for use with MCNP to allow for sampling of uncertainties in any number of input parameters, execution of multiple cases using the uncertainty input parameters, and computation of the resultant uncertainty based on the variation observed in these cases. mcACE was applied in a re-analysis of the AGC-1 experiment. Seven parameters were sampled according to their uncertainties, either known or reasonably estimable: fuel enrichment, control shim angle, uranium cross sections, aluminum density, beryllium density, fuel density, and plate thickness. Among these, the uranium cross-section uncertainties dominated the overall uncertainty, which was small—on the order of 1–2% over most of the range of the energy spectrum.

These MCNP uncertainties produced by the mcACE analysis were used to re-run STAYSL using previously measured AGC-1 data and otherwise identical inputs. Because these uncertainties were so small (smaller even than those associated with the four flux wire activities in each sample), the flux wire measurements were almost irrelevant other than to scale the MCNP spectrum. The composite uncertainty was considerably reduced. This may be expected, but the actual results changed as well in an incongruously and statistically significant way. This is a probable indication that the seven parameters varied in the present analysis are not the origin of the model uncertainty. Sensitivity analysis may help identify more significant contributors in the future.

The spectral adjustment procedure would also benefit from the addition of more activation product data, which would serve to make the result more a product of measurements than primarily models. A series of numerical experiments described herein, with differing subsets of AGC-1 activation data, demonstrated that each additional data point had a significant impact on the final result, an effect that we presume continues to some degree beyond the 4–5 data points obtained in AGC-1. To verify this presumption, an expanded set of ten flux wires has been identified to provide meaningful additional data in irradiations like AGC-1, where the wires cannot be counted for some months following the irradiation. These have now been irradiated in High Flux Isotope Reactor (HFIR). Upon receipt of the activation data, similar numerical experiments could ascertain the impact of data provided by each flux wire. Potential difficulties, such as counting of (relatively) short-lived isotopes and those activation products that are themselves burned up significantly during the irradiation, can be assessed using these data.

Uncertainties in the flux wire measurements themselves also influence the final result, and while these were initially thought to be well characterized and relatively small (~2–3%), it was discovered somewhat by accident that the activity of the same wire measured at different laboratories could differ by significantly more than the reported uncertainty. This prompted two subsequent series of comparative counts using wires drawn from AGC-3, AGC-2, and the Advanced Gas Reactor (AGR-2) experiments involving four laboratories, to ascertain whether this was an isolated or reproducible result, or if it was characteristic of a particular laboratory. The resultant measurements have not yet provided the desired clarity. The first series produced fewer direct comparisons than had been intended for a variety of reasons described above. The measurements varied between laboratories by more than the stated measurement uncertainty in many cases, but without a clear quantitative or qualitative trend between laboratories. The second series produced measurements that differed consistently between two laboratories, but by almost a

factor of two, which was far greater than in any of the earlier comparisons. The differences observed in all cases indicate a clear need to scrutinize the measurement processes at all laboratories in the future.

Finally, a subsequent series of flux wire irradiations in HFIR are planned that should help address all of the above issues. HFIR provides a test case for mcACE that lacks the significant complication of used fuel shuffling, and the expanded flux wire set (presumably refined as the campaign progresses) will be used in conjunction with this to further refine the spectral adjustment process. The wires irradiated will additionally provide further material for the improvement of measurement procedures.

8. REFERENCES

[1] B. Krzykacz, E. Hofer, M. Kloos, "A Software System for Probabilistic Uncertainty and Sensitivity Analysis of Results from Computer Models," Proc. International Conference on Probabilistic Safety Assessment and Management (PSAM-II), San Diego, Ca., USA, (1994).

[2] L. R. Greenwood and C. D. Johnson, "User Guide for the STAYSL PNNL Suite of Software Tools," PNNL-22253, February 2013.TSR-186-5, "Section 5 – Administrative Controls – Technical Safety Requirements for the Advanced Test Reactor," Rev. 16, July 26, 2016.

[3] "International Reactor Dosimetry File 2002 (IRDF-2002), Technical Reports Series No. 452, IAEA, Vienna, Austria, 2006.

[4] J. R. Parry, "As-Run Physics Analysis for the AGC-2 Experiment Irradiated in the ATR," ECAR-2291, March 6, 2014.

[5] P. W. Humrickhouse, "AGC-2 flux wire analysis and radiation damage estimates," INL/EXT-15-35830, 2016.A.G. Croff, "A User's Manual for the ORIGEN2 Computer Code," ORNL/TM-7175, July 1980.

[6] TENDL-2015, "Nuclear Data Library", January 18, 2016.

[7] L. R. Greenwood, "Analysis of AGC-1 Neutron Fluence Monitors," PNNL Project 23747, August 2012.F. Brown, B. Kiedrowsky, J. Bull, et al, "Verification of MCNP-1.60," LA-UR-10-05611 (2010).

[8] Rochman, Dimitri, et al. "Efficient use of Monte Carlo: uncertainty propagation." Nuclear Science and Engineering 177.3 (2014): 337-349.

[9] B. Krzykacz, E. Hofer, M. Kloos, "International Conference on the Physics of Reactors 2012 (PHYSOR 2012)- Advances in Reactor Physics," Knoxville, Tennessee, USA, (15-20 April 2012, Volume 4 of 5).

[10] MCNP6 Users manual-Code version 6.1.1beta, June 2014. LA-CP-14-00745, Los Alamos National Laboratory.

[11] Goorley, J.T., et al., "Initial MCNP6 Release Overview-MCNP6 version 1.0," LA-UR-13-22934, Los Alamos National Laboratory, 2013.

[12] "Verification and Validation Testing of MCNP and ORIGEN2 Computer Codes for Idaho National Laboratory (INL) High Performance computing (HPC) Systems," TEV-2944, Rev. 3, Idaho National Laboratory, 12/18/2018.

[13] ECAR-1406 R0, "As-Run Analysis of the AGC-1 Experiment Irradiated in the ART South Flux Trap", March 22, 2011.

[14] SPC-415, 'Specification for Advanced Test Reactor Mark VII Zone Loaded Fuel Elements', Rev. 03, 09/26/2013.

[15] R. E. MacFarlane and A. C. Kahler, "Methods for Processing ENDF/B-VII with NJOY," Nuclear Data Sheets 111 (2010): 2739-2890.

[16] A. Trkov, M. Herman, and D. A. Brown (eds.), "ENDF-6 Formats Manual, data formats and procedures for the evaluated nuclear data files ENDF/B-VI and ENDF/B-VII," CSEWG Document ENDF-102, BNL-90365-2009 rev. 2, 2012.

[17] D. Rochman, A. Vasiliev, H. Ferroukhi, January 2016, 'Nuclear data uncertainty for criticality-safety: Monte Carlo vs. linear perturbation', Annals of Nuclear Energy 92 (2016) 150-160.

[18] T. Holschuh, W. Windes, J. Navarro, A. Conant, "Impact of Flux Wire Selection on Neutron Spectrum Adjustment," August 2021.

[19] J. Brookman, P. Humrickhouse, V. Patel, and W. Windes, "AGC Uncertainty Analysis," September 2019.

9. Appendix A—Burnup Sensitivity Parameter Fuel Isotopes Investigated

Zr096 Zr094 Zr092 Zr091 Zr090 Y091 Y090

Y089
Xe136
Xe135
Xe134
Xe133
Xe132
Xe131
Xe130
Xe129
Xe128
U240
U239
U238
U237
U235
U233
U234
U232
Tm171
Tm170
Tm169
Th233
Th230
Te132
Te130
Te128
Te126
Te125
Te124
Te123
Te122
Tc099
Tb161
Tb160
Tb159
Ta182
Ta181
Sr090
Sr089
Sr088
Sr087
Sn126
Sn125
Sn124
Sn122
Sn120
Sn119
Sn118
Sn117
Sn116
Sn115
Sn114
Sn112
Sm154
Sm153
Sm152
Sm151
Sm150
Sm149
Sm148
Sm147
Si031
Se082
Se080
Se079
Se078
Se077
Sb127
Sb126
Sb125
Sb124
Sb123
Sb121
Ru106
Ru105
Ru104
Ru103
Ru102
Ru101
Ru100
Rh105
Rh103
Rb087
Rb086
Rb085
Pu243
Pu242
Pu240
Pu239
Pu238
Pu237
Pu236
Pt195
Pr143
Pr142
Pr141
Pm151
Pm149
Pm148
Pm147
Pd110
Pd108
Pd107
Pd106
Pd105
Pd104
Pb208
Pb207
Pb206
Pa234
Pa233
Pa232
Pa231
O016
Np239
Np238
Np237
Np236
Ni064
Ni062
Ni061
Ni060
Ni059
Ni058
Nd150
Nd148
Nd147
Nd146
Nd145
Nd144
Nd143
Nd142
Nb095
Nb093
Na023
Mo100
Mo098
Mo097
Mo096
Mo095
Mo094
Mo092
Mn055
Lu176
Lu175
Li006
La140
La139
Kr086
Kr085
Kr084
Kr083
Kr082
Ir193
Ir191
In115
In113
I135
I131
I130
I129
I127
Ho165
Hf180
Hf179
Hf178
Hf177
Hf176
Hf175
Hf174
He004
H2
H1
Ge077
Ge076
Gd160
Gd158
Gd157
Gd156
Gd155
Gd154
Gd153
Gd152
Fe058
Fe057
Fe056
Fe054
F019
Eu157
Eu156
Eu154
Eu153
Eu152
Eu151
Er170
Er168
Er167
Er166
Er164
Er162
Dy164
Dy162
Dy161
Dy160
Cu065
Cu064
Cu063
Cs137
Cs136
Cs135
Cs134
Cs133
Cr053
Cr052
Cr050
Co059
Cm248
Cm247
Cm246
Cm245
Cm244
Cm243
Cm242
Cf252
Cf251
Cf250
Cf249
Ce144
Ce143
Ce142
Ce141
Ce140
Cd116
Cd114
Cd113
Cd112
Cd111
Cd110
Br081
Bk249
Bi209
Be009
Ba140
Ba138
Ba137
Ba136
Ba135
Ba134
B011
B010
Au197
Am243
Am242
Am241
Al027
Ag109
Ag107

10. Appendix B

Uncertainty Quantification Results: All Input Parameters Analyzed Simultaneously

Tally Elevation from Core Midplane (cm)	-53.98		-34.93		-18.42		5.72		17.78		31.75		46.99	
Energy (MeV)	error	value	error	value	error	value	error	value	error	value	error	value	error	value
1.00E-10	0	0	0	0	0	0	0	0	0	0	0	0	0	0
1.00E-09	5.19E-10	2.28E-09	4.10E-10	3.99E-09	6.18E-10	5.27E-09	8.59E-11	5.20E-09	1.00E-09	4.80E-09	6.31E-10	3.80E-09	3.51E-10	2.02E-09
1.00E-08	4.26E-09	3.72E-07	5.23E-09	6.88E-07	1.38E-08	8.66E-07	2.07E-08	8.84E-07	7.94E-09	7.98E-07	3.68E-09	6.18E-07	3.39E-09	3.34E-07
2.30E-08	5.89E-09	1.36E-06	1.82E-08	2.53E-06	4.12E-08	3.18E-06	1.44E-08	3.28E-06	2.14E-08	2.96E-06	2.64E-08	2.30E-06	2.34E-08	1.24E-06
5.00E-08	7.31E-09	3.55E-06	3.27E-08	6.60E-06	4.33E-08	8.35E-06	3.11E-08	8.64E-06	3.86E-08	7.84E-06	4.48E-08	6.12E-06	2.90E-08	3.31E-06
7.60E-08	2.90E-08	2.70E-06	9.42E-09	5.05E-06	3.57E-08	6.39E-06	2.66E-08	6.62E-06	2.45E-08	6.02E-06	4.20E-08	4.71E-06	3.21E-08	2.56E-06
1.15E-07	2.47E-08	2.50E-06	3.23E-08	4.70E-06	4.13E-08	5.95E-06	2.32E-08	6.16E-06	2.44E-08	5.60E-06	3.90E-08	4.39E-06	1.31E-08	2.40E-06
1.70E-07	1.41E-09	1.69E-06	2.53E-08	3.22E-06	3.84E-08	4.07E-06	2.00E-08	4.21E-06	3.23E-08	3.84E-06	9.42E-09	3.01E-06	3.95E-08	1.67E-06
2.55E-07	1.81E-08	1.11E-06	1.07E-08	2.15E-06	1.07E-08	2.71E-06	2.09E-08	2.81E-06	2.64E-08	2.57E-06	1.94E-08	2.03E-06	7.52E-09	1.14E-06
3.80E-07	8.41E-09	7.67E-07	1.98E-08	1.50E-06	6.82E-09	1.89E-06	1.67E-08	1.97E-06	2.07E-08	1.80E-06	2.56E-08	1.43E-06	1.68E-08	8.30E-07
5.50E-07	8.26E-09	6.19E-07	2.26E-08	1.20E-06	1.22E-08	1.51E-06	2.07E-08	1.58E-06	2.37E-08	1.45E-06	1.07E-08	1.15E-06	2.01E-09	6.77E-07
8.40E-07	1.53E-08	6.58E-07	2.71E-08	1.28E-06	2.15E-08	1.62E-06	1.68E-08	1.69E-06	1.04E-08	1.55E-06	1.62E-08	1.23E-06	1.99E-08	7.30E-07
1.28E-06	2.20E-08	6.23E-07	2.25E-08	1.22E-06	2.28E-08	1.52E-06	2.68E-08	1.58E-06	1.37E-08	1.45E-06	1.19E-08	1.16E-06	1.23E-08	6.86E-07
1.90E-06	1.11E-08	5.78E-07	2.36E-08	1.13E-06	1.22E-08	1.43E-06	1.74E-08	1.49E-06	2.12E-08	1.36E-06	2.48E-08	1.09E-06	2.04E-08	6.47E-07
2.80E-06	1.30E-08	5.52E-07	1.10E-08	1.07E-06	2.09E-08	1.35E-06	2.23E-08	1.42E-06	2.07E-08	1.31E-06	1.55E-08	1.05E-06	1.60E-08	6.26E-07
4.25E-06	1.60E-08	5.94E-07	1.31E-08	1.16E-06	3.41E-09	1.46E-06	1.47E-08	1.53E-06	2.55E-08	1.41E-06	1.31E-08	1.13E-06	1.78E-08	6.73E-07
6.30E-06	1.04E-08	5.46E-07	1.86E-08	1.06E-06	2.77E-08	1.34E-06	1.88E-08	1.40E-06	2.48E-08	1.30E-06	2.43E-08	1.04E-06	1.63E-08	6.21E-07
9.20E-06	2.63E-09	5.27E-07	9.74E-09	1.03E-06	3.62E-08	1.29E-06	9.95E-09	1.35E-06	1.24E-08	1.25E-06	1.28E-08	1.00E-06	8.40E-09	6.01E-07

Tally Elevation from Core Midplane (cm)	-53.98		-34.93		-18.42		5.72		17.78		31.75		46.99	
1.35E-05	9.06E-09	5.39E-07	1.58E-08	1.05E-06	4.27E-09	1.31E-06	8.44E-09	1.37E-06	1.19E-08	1.26E-06	2.41E-08	1.01E-06	5.12E-09	6.03E-07
2.10E-05	1.74E-08	6.17E-07	6.96E-09	1.21E-06	1.88E-08	1.51E-06	3.60E-08	1.58E-06	6.30E-09	1.46E-06	8.03E-09	1.18E-06	1.14E-08	7.09E-07
3.00E-05	1.33E-08	4.99E-07	1.21E-08	9.79E-07	2.65E-08	1.23E-06	1.41E-08	1.28E-06	7.40E-09	1.19E-06	3.48E-09	9.58E-07	1.76E-08	5.75E-07
4.50E-05	1.91E-08	5.76E-07	1.93E-08	1.11E-06	2.07E-08	1.40E-06	5.48E-09	1.47E-06	1.87E-08	1.36E-06	1.45E-08	1.09E-06	9.13E-09	6.60E-07
6.90E-05	1.57E-08	6.06E-07	2.44E-08	1.18E-06	6.49E-09	1.48E-06	1.29E-08	1.55E-06	2.08E-08	1.43E-06	9.39E-09	1.14E-06	6.47E-09	6.94E-07
0.0001	3.66E-09	5.26E-07	1.94E-08	1.03E-06	9.67E-09	1.28E-06	1.98E-08	1.34E-06	8.31E-09	1.24E-06	8.26E-09	1.00E-06	1.22E-08	6.01E-07
0.000135	8.61E-09	4.28E-07	2.01E-08	8.28E-07	2.12E-08	1.04E-06	1.95E-08	1.09E-06	1.16E-08	1.00E-06	4.71E-09	8.09E-07	1.22E-08	4.88E-07
0.00017	4.65E-09	3.25E-07	1.08E-08	6.38E-07	1.52E-08	7.99E-07	1.38E-08	8.37E-07	1.52E-08	7.71E-07	8.07E-09	6.19E-07	9.59E-09	3.80E-07
0.00022	9.32E-09	3.66E-07	5.61E-09	7.12E-07	1.62E-08	8.94E-07	1.69E-08	9.39E-07	1.42E-08	8.66E-07	1.45E-08	6.97E-07	7.57E-09	4.24E-07
0.00028	4.77E-09	3.41E-07	8.60E-09	6.64E-07	1.14E-08	8.35E-07	1.54E-08	8.79E-07	1.92E-08	8.09E-07	5.74E-09	6.52E-07	8.77E-09	3.95E-07
0.00036	5.99E-09	3.54E-07	1.87E-08	6.94E-07	1.09E-08	8.72E-07	1.69E-08	9.10E-07	1.28E-08	8.42E-07	1.35E-08	6.76E-07	1.07E-08	4.10E-07
0.00045	1.33E-08	3.15E-07	1.50E-08	6.17E-07	1.58E-08	7.72E-07	1.75E-08	8.13E-07	1.58E-08	7.46E-07	9.96E-09	6.02E-07	2.30E-09	3.65E-07
0.000575	8.82E-09	3.45E-07	8.85E-09	6.74E-07	1.83E-08	8.48E-07	9.31E-09	8.96E-07	2.18E-08	8.19E-07	1.24E-08	6.63E-07	1.07E-08	3.98E-07
0.00076	9.97E-09	3.95E-07	1.55E-08	7.68E-07	2.12E-08	9.65E-07	1.17E-08	1.02E-06	5.04E-09	9.34E-07	9.33E-09	7.52E-07	7.51E-09	4.59E-07
0.00096	8.36E-09	3.30E-07	2.20E-09	6.45E-07	1.00E-08	8.09E-07	1.72E-08	8.47E-07	8.25E-09	7.83E-07	1.90E-08	6.30E-07	1.02E-08	3.83E-07
0.001275	8.88E-09	4.01E-07	1.16E-08	7.82E-07	1.08E-08	9.78E-07	2.94E-08	1.03E-06	6.93E-09	9.48E-07	9.68E-09	7.67E-07	1.02E-08	4.66E-07
0.0016	1.09E-08	3.25E-07	1.30E-08	6.36E-07	2.47E-08	7.96E-07	9.63E-09	8.35E-07	1.66E-08	7.73E-07	1.37E-08	6.19E-07	8.88E-09	3.82E-07
0.002	9.43E-09	3.23E-07	4.53E-09	6.30E-07	1.53E-08	7.89E-07	5.62E-09	8.28E-07	1.81E-08	7.66E-07	1.05E-08	6.14E-07	5.70E-09	3.74E-07
0.0027	1.31E-08	4.34E-07	9.61E-09	8.52E-07	1.92E-08	1.07E-06	1.09E-08	1.11E-06	1.16E-08	1.03E-06	1.42E-08	8.30E-07	9.65E-09	5.04E-07
0.0034	9.69E-09	3.36E-07	4.46E-09	6.58E-07	7.26E-09	8.23E-07	2.36E-08	8.56E-07	1.30E-08	7.94E-07	1.45E-08	6.44E-07	3.24E-09	3.92E-07
0.0045	1.22E-08	4.04E-07	1.51E-09	7.87E-07	1.95E-08	9.86E-07	1.47E-08	1.03E-06	4.24E-09	9.53E-07	1.84E-08	7.74E-07	1.90E-09	4.66E-07
0.0055	5.59E-09	2.89E-07	1.57E-08	5.63E-07	2.01E-08	7.10E-07	6.35E-09	7.40E-07	2.25E-08	6.86E-07	8.74E-09	5.49E-07	1.20E-08	3.32E-07
0.0072	2.82E-09	3.88E-07	2.71E-08	7.54E-07	1.95E-08	9.52E-07	1.37E-08	9.91E-07	2.19E-08	9.13E-07	1.87E-08	7.35E-07	1.81E-08	4.49E-07
0.0092	8.39E-09	3.47E-07	1.25E-08	6.79E-07	2.04E-08	8.48E-07	2.39E-08	8.87E-07	1.51E-08	8.18E-07	1.72E-08	6.65E-07	1.02E-08	4.03E-07
0.012	1.29E-08	4.01E-07	9.71E-09	7.83E-07	4.56E-09	9.79E-07	1.40E-08	1.03E-06	2.51E-08	9.59E-07	5.98E-09	7.80E-07	6.62E-09	4.72E-07

Tally Elevation from Core Midplane (cm)	-53.98		-34.93		-18.42		5.72		17.78		31.75		46.99	
0.015	1.31E-08	3.45E-07	1.72E-08	6.66E-07	5.66E-09	8.43E-07	2.33E-08	8.74E-07	1.37E-08	8.09E-07	1.13E-08	6.49E-07	1.48E-08	3.96E-07
0.019	7.87E-09	3.64E-07	9.41E-09	7.06E-07	1.64E-08	8.83E-07	1.78E-08	9.15E-07	2.36E-08	8.40E-07	1.14E-08	6.72E-07	6.12E-10	4.02E-07
0.0255	7.67E-09	4.82E-07	1.16E-08	9.31E-07	1.52E-08	1.17E-06	1.60E-08	1.22E-06	1.48E-08	1.13E-06	1.05E-08	9.05E-07	8.82E-09	5.48E-07
0.032	6.30E-09	3.53E-07	1.26E-08	6.89E-07	9.60E-09	8.68E-07	1.34E-08	9.02E-07	8.46E-10	8.32E-07	1.87E-08	6.69E-07	2.47E-09	4.04E-07
0.04	4.88E-09	3.55E-07	9.03E-09	6.97E-07	9.63E-09	8.77E-07	8.46E-09	9.14E-07	2.38E-08	8.45E-07	2.06E-08	6.78E-07	7.15E-09	4.10E-07
0.0525	9.67E-09	4.98E-07	1.37E-08	9.70E-07	8.23E-09	1.21E-06	9.88E-09	1.27E-06	1.67E-08	1.18E-06	7.27E-09	9.45E-07	1.30E-08	5.70E-07
0.066	4.37E-09	4.48E-07	1.20E-08	8.77E-07	5.87E-09	1.10E-06	2.40E-08	1.15E-06	2.43E-08	1.07E-06	2.49E-08	8.59E-07	1.64E-08	5.21E-07
0.088	1.61E-08	5.88E-07	1.59E-08	1.15E-06	1.25E-08	1.44E-06	3.25E-08	1.50E-06	1.94E-08	1.38E-06	7.20E-09	1.11E-06	1.70E-08	6.76E-07
0.11	1.27E-08	4.82E-07	1.57E-08	9.42E-07	1.03E-08	1.18E-06	7.55E-09	1.24E-06	2.17E-08	1.14E-06	1.38E-08	9.19E-07	1.57E-08	5.53E-07
0.135	1.64E-08	5.07E-07	1.69E-08	9.84E-07	1.11E-08	1.23E-06	1.27E-08	1.29E-06	2.19E-08	1.19E-06	1.49E-08	9.64E-07	1.09E-08	5.81E-07
0.16	1.58E-08	4.04E-07	7.00E-09	7.86E-07	2.19E-08	9.82E-07	1.24E-08	1.03E-06	1.07E-08	9.51E-07	1.28E-08	7.70E-07	9.30E-09	4.65E-07
0.19	5.50E-09	4.63E-07	1.19E-08	9.05E-07	1.44E-08	1.13E-06	9.13E-09	1.18E-06	2.03E-08	1.09E-06	1.83E-08	8.75E-07	1.90E-08	5.37E-07
0.22	1.75E-08	4.13E-07	1.11E-08	8.03E-07	2.52E-08	1.00E-06	2.05E-08	1.06E-06	2.34E-08	9.75E-07	1.13E-08	7.87E-07	1.64E-08	4.70E-07
0.255	3.95E-09	4.57E-07	1.20E-08	8.87E-07	6.85E-09	1.11E-06	1.73E-08	1.17E-06	1.75E-08	1.07E-06	8.18E-09	8.69E-07	1.48E-08	5.23E-07
0.29	1.10E-08	4.20E-07	2.00E-08	8.21E-07	6.93E-09	1.02E-06	7.97E-09	1.08E-06	2.26E-08	9.89E-07	1.51E-08	7.97E-07	1.45E-08	4.87E-07
0.32	1.89E-08	3.26E-07	1.11E-08	6.32E-07	1.20E-08	7.85E-07	1.58E-08	8.27E-07	1.16E-08	7.64E-07	2.07E-08	6.17E-07	9.59E-09	3.76E-07
0.36	5.57E-09	4.15E-07	1.14E-08	8.04E-07	2.73E-08	1.01E-06	1.03E-08	1.05E-06	8.22E-09	9.79E-07	1.38E-09	7.87E-07	6.90E-09	4.80E-07
0.4	1.21E-08	3.69E-07	1.86E-08	7.21E-07	5.71E-09	9.01E-07	1.97E-08	9.43E-07	2.47E-08	8.69E-07	4.48E-09	7.00E-07	8.00E-09	4.26E-07
0.45	1.23E-08	4.05E-07	1.72E-08	7.88E-07	8.92E-09	9.88E-07	1.88E-08	1.03E-06	9.54E-09	9.55E-07	1.20E-08	7.66E-07	7.50E-09	4.66E-07
0.5	7.38E-09	4.10E-07	1.31E-08	7.97E-07	1.96E-08	9.97E-07	2.50E-08	1.05E-06	7.56E-09	9.66E-07	1.14E-08	7.78E-07	1.99E-08	4.73E-07
0.55	9.70E-09	3.93E-07	1.05E-08	7.60E-07	1.07E-08	9.51E-07	1.36E-08	9.99E-07	1.92E-08	9.22E-07	8.88E-09	7.41E-07	1.08E-08	4.52E-07
0.6	6.37E-09	3.67E-07	1.00E-08	7.07E-07	2.31E-08	8.89E-07	1.83E-08	9.33E-07	1.47E-08	8.65E-07	1.27E-08	7.03E-07	7.85E-09	4.27E-07
0.66	1.28E-08	4.19E-07	1.83E-08	8.08E-07	1.16E-08	1.01E-06	1.21E-08	1.06E-06	1.59E-08	9.84E-07	1.15E-08	7.90E-07	8.61E-09	4.84E-07
0.72	8.43E-09	4.07E-07	1.49E-08	7.84E-07	2.15E-08	9.78E-07	2.41E-08	1.03E-06	1.21E-08	9.52E-07	1.18E-08	7.68E-07	5.28E-09	4.64E-07
0.78	1.48E-08	3.71E-07	1.46E-08	7.17E-07	1.43E-08	9.03E-07	8.81E-09	9.51E-07	1.54E-08	8.73E-07	1.22E-08	7.03E-07	1.13E-08	4.32E-07

Tally Elevation from Core Midplane (cm)	-53.98		-34.93		-18.42		5.72		17.78		31.75		46.99	
0.84	1.07E-08	3.25E-07	1.30E-08	6.21E-07	1.65E-08	7.85E-07	2.19E-08	8.19E-07	1.20E-08	7.57E-07	4.46E-09	6.12E-07	1.89E-09	3.75E-07
0.92	8.57E-09	3.99E-07	1.79E-08	7.64E-07	2.71E-08	9.64E-07	1.02E-08	1.01E-06	3.91E-09	9.32E-07	1.28E-08	7.53E-07	8.49E-09	4.60E-07
1	1.01E-08	3.68E-07	2.50E-08	7.07E-07	9.24E-09	8.83E-07	2.14E-08	9.24E-07	1.39E-08	8.56E-07	1.63E-08	6.92E-07	1.41E-08	4.16E-07
1.2	1.61E-08	8.43E-07	3.00E-08	1.62E-06	4.49E-08	2.03E-06	4.38E-08	2.13E-06	4.32E-08	1.97E-06	2.46E-08	1.59E-06	2.81E-08	9.64E-07
1.4	1.32E-08	7.47E-07	1.82E-08	1.45E-06	3.97E-08	1.80E-06	3.05E-08	1.89E-06	2.79E-08	1.74E-06	1.21E-08	1.41E-06	1.86E-08	8.56E-07
1.6	2.16E-08	6.56E-07	2.20E-08	1.26E-06	4.78E-08	1.58E-06	4.02E-08	1.65E-06	4.24E-08	1.53E-06	4.05E-08	1.23E-06	2.57E-08	7.47E-07
1.8	3.16E-09	5.63E-07	1.67E-08	1.09E-06	4.54E-08	1.36E-06	4.92E-08	1.43E-06	3.53E-08	1.32E-06	2.36E-08	1.06E-06	1.05E-08	6.43E-07
2	1.91E-08	4.95E-07	3.44E-08	9.52E-07	4.71E-08	1.20E-06	3.25E-08	1.25E-06	3.59E-08	1.15E-06	3.48E-08	9.34E-07	2.48E-08	5.61E-07
2.3	3.12E-08	6.11E-07	5.23E-08	1.17E-06	6.90E-08	1.46E-06	6.85E-08	1.52E-06	6.80E-08	1.41E-06	5.92E-08	1.13E-06	2.71E-08	6.90E-07
2.6	2.25E-08	5.26E-07	5.29E-08	1.00E-06	5.84E-08	1.26E-06	7.85E-08	1.32E-06	6.67E-08	1.22E-06	5.76E-08	9.80E-07	4.27E-08	6.01E-07
2.9	2.41E-08	3.70E-07	4.09E-08	7.08E-07	5.38E-08	8.86E-07	5.69E-08	9.23E-07	5.86E-08	8.60E-07	5.18E-08	6.92E-07	2.55E-08	4.22E-07
3.3	3.13E-08	3.53E-07	5.22E-08	6.68E-07	7.16E-08	8.39E-07	6.73E-08	8.75E-07	7.03E-08	8.09E-07	5.28E-08	6.48E-07	3.30E-08	3.99E-07
3.7	2.23E-08	2.19E-07	4.14E-08	4.21E-07	4.92E-08	5.24E-07	5.81E-08	5.51E-07	5.02E-08	5.11E-07	4.38E-08	4.12E-07	2.50E-08	2.50E-07
4.1	2.36E-08	1.90E-07	4.00E-08	3.61E-07	5.43E-08	4.51E-07	5.75E-08	4.72E-07	5.42E-08	4.33E-07	4.40E-08	3.53E-07	2.79E-08	2.15E-07
4.5	2.08E-08	1.53E-07	4.03E-08	2.91E-07	5.08E-08	3.64E-07	5.48E-08	3.81E-07	4.39E-08	3.51E-07	3.85E-08	2.84E-07	2.43E-08	1.71E-07
5	2.18E-08	1.55E-07	4.45E-08	2.93E-07	6.11E-08	3.68E-07	6.20E-08	3.85E-07	5.26E-08	3.56E-07	4.56E-08	2.83E-07	2.96E-08	1.75E-07
5.5	2.15E-08	1.06E-07	3.58E-08	1.99E-07	4.31E-08	2.51E-07	4.59E-08	2.60E-07	4.27E-08	2.41E-07	3.51E-08	1.93E-07	2.28E-08	1.20E-07
6	1.60E-08	7.27E-08	2.87E-08	1.39E-07	3.56E-08	1.74E-07	3.70E-08	1.82E-07	3.34E-08	1.69E-07	2.69E-08	1.36E-07	1.82E-08	8.29E-08
6.7	1.66E-08	6.60E-08	2.87E-08	1.23E-07	3.71E-08	1.57E-07	3.81E-08	1.62E-07	3.45E-08	1.51E-07	2.92E-08	1.21E-07	1.71E-08	7.51E-08
7.4	1.04E-08	4.22E-08	2.19E-08	7.93E-08	2.82E-08	9.94E-08	2.97E-08	1.04E-07	2.50E-08	9.68E-08	2.15E-08	7.96E-08	1.35E-08	4.90E-08
8.2	7.67E-09	2.36E-08	1.48E-08	4.53E-08	1.70E-08	5.61E-08	1.75E-08	5.93E-08	1.69E-08	5.46E-08	1.36E-08	4.37E-08	7.89E-09	2.75E-08
9	4.05E-09	1.47E-08	1.07E-08	2.85E-08	1.24E-08	3.49E-08	1.37E-08	3.69E-08	1.26E-08	3.38E-08	9.44E-09	2.71E-08	6.00E-09	1.69E-08
10	3.39E-09	9.56E-09	6.81E-09	1.78E-08	1.03E-08	2.29E-08	9.17E-09	2.39E-08	8.98E-09	2.25E-08	6.66E-09	1.79E-08	4.93E-09	1.08E-08
11	2.44E-09	4.86E-09	3.98E-09	8.82E-09	6.75E-09	1.13E-08	5.78E-09	1.25E-08	4.71E-09	1.14E-08	5.05E-09	9.02E-09	2.67E-09	5.50E-09
12	0	0	0	2.08E-09	2.20E-09	5.16E-09	1.38E-09	5.11E-09	3.08E-09	4.95E-09	0	0	0	0

Tally Elevation from Core Midplane (cm)	-53.98		-34.93		-18.42		5.72		17.78		31.75		46.99	
13	0	0	0	0	0	0	0	0	0	0	0	0	0	0
14	0	0	0	0	0	0	0	0	0	0	0	0	0	0
15	0	0	0	0	0	0	0	0	0	0	0	0	0	0
16	0	0	0	0	0	0	0	0	0	0	0	0	0	0
17	0	0	0	0	0	0	0	0	0	0	0	0	0	0
18	0	0	0	0	0	0	0	0	0	0	0	0	0	0
19	0	0	0	0	0	0	0	0	0	0	0	0	0	0
20	0	0	0	0	0	0	0	0	0	0	0	0	0	0
1000000	4.47E-07	4.67E-05	7.26E-07	8.99E-05	8.45E-07	0.0001129	1.01E-06	0.0001178	1.01E-06	0.0001083	8.83E-07	8.64E-05	6.74E-07	5.09E-05